

Cosmic Rays VI

Starburst Galaxies at multiwavelengths

Julia K. Becker^{1,2,*}, Peter L. Biermann^{3,4,5,6,7}, Jens Dreyer², and Tanja M. Kneiske^{2,8}

¹ Göteborgs Universitet, Institutionen för Fysik, 41296 Göteborg, Sweden

² Technische Universität Dortmund, Institut für Physik, D-44221 Dortmund, Germany

³ MPI for Radioastronomy, Auf dem Hügel 69, D-53121 Bonn, Germany

⁴ Dept. of Phys. & Astron., Univ. of Bonn, Germany

⁵ Dept. of Phys. & Astron., Univ. of Alabama, Tuscaloosa, AL, USA

⁶ Dept. of Phys. & Astron., Univ. of Alabama, Huntsville, AL, USA

⁷ Inst. Nucl. Phys. FZ, Karlsruhe Inst. of Techn. (KIT), Karlsruhe, Germany

⁸ University of Hamburg, Institut für Experimentalphysik, Hamburg, Germany

November 5, 2018

ABSTRACT

Context. Starburst galaxies show a direct correlation between radio and far-infrared emission. High target densities and a high rate of supernova explosions imply the possibility of accelerating hadronic cosmic rays and producing decay products from hadronic interactions, like high-energy neutrinos and photons.

Aims. We propose an explanation for the far-infrared/radio correlation of galaxies in terms of the energy balance of the interstellar medium and determine the flux from high-energy photons and neutrinos from starburst galaxies.

Methods. We present a catalog of the 127 brightest starburst galaxies with redshifts of $z < 0.03$. In order to investigate the correlation between radio- and far-infrared emission, we apply the leaky box approximation. Further, we derive photon- and neutrino spectra from proton-proton interactions in supernova remnants (SNRs). Here, we assume that a fraction of the SNR's energy is transferred to the acceleration of cosmic rays. We also investigate the possibility of detecting Gamma Ray Bursts from nearby starburst galaxies, using the catalog defined here.

Results. We show that the radio emission is only weakly dependent on the magnetic field. It turns out that the intensity of the radio signal is directly proportional to the number of supernova explosions, which scales with the far-infrared luminosity. In addition, we find that high-energy photons from proton-proton interactions in SNRs in starbursts can make up several percent of the diffuse gamma-ray background. The neutrino flux from the same sources has a maximum energy of $\sim 10^5$ GeV. Neutrinos can, on the other hand, be observed if a Gamma Ray Burst happens in a nearby starburst. About 0.03 GRBs per year are expected to occur in the entire catalog. The true number is expected to be even higher, since we only include the brightest sources. The number of events per burst in IceCube varies between about one event and more than 1000 events. This provides good prospects for IceCube to detect a significant event, since the background for a GRB search is close to zero.

Key words. Galaxies: starburst – Infrared: galaxies – Radio continuum: galaxies – Catalogs – cosmic rays – Neutrinos

1. Introduction

Radio emission from galaxies is usually dominated by synchrotron emission from a population of non-thermal, energetic electrons in a magnetic field which permeates most of the interstellar medium. This radio emission is often spatially structured, such as in the starburst galaxy M82, showing individual compact sources, which can be interpreted as fairly young supernova remnants (Kronberg et al., 1985; Kronberg & Sramek, 1985; Bartel et al., 1987). The origin of these energetic electrons, a part of the cosmic rays, is thus expected to be the young supernova remnants, see Baade & Zwicky (1934); Shklovskii (1953) and for an extensive review Berezhinsky et al. (1990). Thus the radio emission is a key to interpret the physics of cosmic rays, and conversely, any attempt to understand cosmic rays should also try to understand the properties of the radio emission.

Galaxies also have abundant far-infrared (FIR) emission, which is due to dust. This dust is heated by stars, often mostly young stars. As was noted from the mid-eighties, this thermal dust emission correlates rather well with the non-thermal radio emission. The correlation in its most simple form is just a proportionality between far-infrared and non-thermal emission. As reference wavelengths, $60\mu\text{m}$ and $100\mu\text{m}$ are used for the far-infrared. Frequencies between 1.4 GHz and 5 GHz are used as typical for the radio regime.

Many attempts have been made to understand the proportionality between radio and far-infrared. On the basis of rather simple modeling of galactic evolution, a strong correlation is actually expected, since both supernova remnants and the dominant heating by ultraviolet light from massive stars derives from the same stellar population (Biermann, 1976; Biermann & Fricke, 1977). Using such models the far-infrared luminosity of NGC2146 had been predicted by Kronberg & Biermann (1981) and verified subsequently by IRAS observations (Moshir et al., 1990a). The correlation as seen in the data was first clearly stated by de Jong et al. (1985), and subsequently discussed at some length

* Corresponding author. Contact: julia.becker@physics.gu.se, phone: +46-31-7723190

by many authors (Bicay et al., 1989; Wunderlich et al., 1987; Wunderlich & Klein, 1988, 1991; Condon et al., 1991). It still defies a clear explanation.

An extensive attempt to interpret the correlation was made by Völk and collaborators (Völk, 1989; Xu et al., 1994b,a; Lisenfeld et al., 1996). The electrons are believed to lose all energy in this model and therefore, the correlation is calorimetric. However, this would predict an actual steepening of the radio emission between the reference frequencies, an effect which is not seen in the data. The solution of a spatial mixture of cutoffs would still allow for a locally loss-dominated scenario. However, first spatially resolved observations of M 33 indicate that the local star-forming regions typically have flat spectra, too (Tabatabaei et al., 2007a,b). It is therefore likely that star forming regions are generally injection dominated.

Here, we propose a simple model, based upon a particular picture of the energy balance in the interstellar medium. This model also uses some simple assumptions, as we will emphasize. The model is local, and so automatically allows for starbursts and gradients in disk galaxies, while upholding the correlation. The model leads to some specific predictions which can be checked with further data. A catalog of starburst galaxies is presented to perform first checks.

The outline of this paper is as follows: We first define variables, used throughout the paper, in Section 2. In Section 3, a catalog of 127 nearby, bright starburst galaxies is presented, including far-infrared, radio and X-ray data. The correlation between FIR and radio emission is outlined together with the difficulty of explaining it. In Section 4, we present a model explaining the FIR-radio correlation. The possible emission of cosmic rays and secondaries produced in proton-proton and proton-photon interactions is discussed in Section 5. In particular, we examine the possibility of detecting secondaries from supernova remnants, as well as cosmic rays and secondaries from Gamma Ray Bursts in starbursts. Finally, implications are discussed in Section 6.

2. Definitions

In the following sections, the electromagnetic spectra at different wavelengths are used in order to investigate the starburst nature of the catalog sources. Table 1 gives a summary of the different parameters used. Concerning spectral power-law fits between the wavelengths, we use the convention

$$S = S_0 \cdot \left(\frac{\nu}{\nu_0} \right)^\alpha, \quad (1)$$

with S as the flux per area and frequency interval, in units of $\text{Jy} = 10^{-26} \text{ W/m}^2/\text{Hz}$. Here, S_0 is the flux at a reference frequency ν_0 .

3. Local starbursts: a sample

In this section, we present a sample of local starburst galaxies¹. The data of the individual sources are presented in appendix A.

¹ The data have been collected from the references (Heeschen & Wade, 1964; Whiteoak, 1970; Sramek, 1975; Sramek & Tovmassian, 1976; Disney & Wall, 1977; Dressel & Condon, 1978; Kühr et al., 1981; Condon et al., 1983; Wright & Otrupcek, 1990; Condon, 1983; Beichman et al., 1988; Soifer et al., 1989; Moshir et al., 1990b; Becker et al., 1991; Fabbiano et al., 1992; White & Becker, 1992; Brinkmann et al., 1994; Knapp, 1994; Wright et al., 1994; Griffith et al., 1994, 1995; Becker et al., 1995; Rigopoulou et al., 1996; Wright et al., 1996;

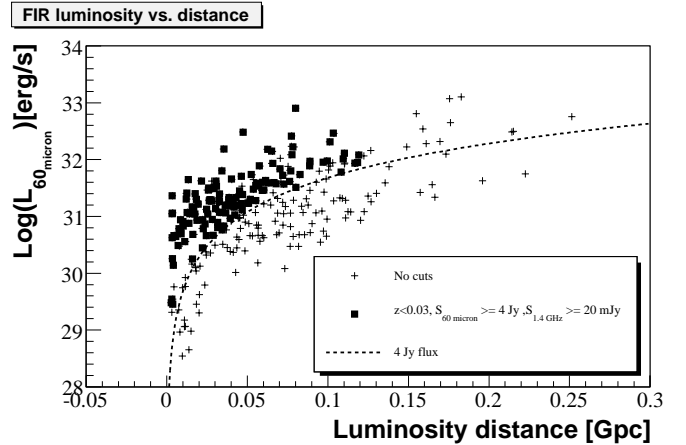


Fig. 1. 60μ luminosity - distance diagram. Crosses indicate all 309 pre-selected starburst galaxies, squares show those remaining after the cuts $S_{1.4\text{GHz}} > 20 \text{ mJy}$ and $S_{60\mu} > 4 \text{ Jy}$ and $z < 0.03$. The dashed line shows the sensitivity for $S_{60\mu} > 4 \text{ Jy}$.

Only local sources are considered, since our aim is to investigate the closest sources. The catalog presented here consists of a total of 127 starburst galaxies. This is a sub-sample from a larger sample of 309 starburst galaxies, applying cuts at both FIR and radio wavelengths to ensure a complete, local sample. These cuts are discussed in the following paragraphs. Different tests were performed in order to verify that the considered galaxies are indeed starbursts, as presented in the following paragraphs. In order to remove contamination from Seyfert galaxies, we only use high ratios of FIR to radio flux density, i.e. $S_{60\mu}/S_{1.4\text{GHz}} > 30$. To test if the sample consists of starburst galaxies as opposed to regular galaxies, we check that the correlation between radio power and FIR luminosity is a direct proportionality. Apart from that, our main criterion for the catalog is that the sources are closer than $z < 0.03$, i.e. located in the supergalactic plane, and that they have both radio and IR detections. The latter gives us information about the ratio of the IR to radio signal, which we require to be larger than 30. This ensures a high IR component compared to the radio part, i.e. that the sources are indeed starbursts and not Seyfert galaxies. Further, we apply sensitivity cuts, we only include sources with a flux density $> 4 \text{ Jy}$ at $60 \mu\text{m}$ and a radio flux density at 1.4 GHz larger than 20 mJy . Figures 1 and 2 show the $60 \mu\text{m}$ resp. 1.4 GHz luminosity of starburst galaxies versus their luminosity distance. The dotted lines represent the sensitivity for 4 Jy , resp. 20 mJy . Crosses represent all 309 sources we selected in the beginning, squares show those 127 sources remaining after the cuts at $S_{1.4\text{GHz}} > 20 \text{ mJy}$ and $S_{60\mu} > 4 \text{ Jy}$, as well as $z < 0.03$. We apply those cuts in order to ensure a complete, local sample in both FIR and radio wavelengths. Since the sources are closer than $z = 0.03$, many of the starbursts are located in the supergalactic plane. Their spatial distribution should therefore be a flat cylinder with a further more spherical component, for those sources not in the supergalactic plane. We therefore expect that the number of sources with a

Douglas et al., 1996; Condon et al., 1996, 1998; White et al., 2000; Condon et al., 2002; Sanders et al., 2003; Strickland et al., 2004; Vollmer et al., 2004; Surace et al., 2004; Bravo-Alfaro et al., 2004; Leroy et al., 2005a; Nagar et al., 2005; Ott et al., 2005; Leroy et al., 2005b; Iono et al., 2005; Tajer et al., 2005; Teng et al., 2005; Guainazzi et al., 2005; Baan & Klöckner, 2006; Tüllmann et al., 2006; Gallimore et al., 2006; Lisenfeld et al., 2007; Rosa-González et al., 2007; Shu et al., 2007)

parameter	symbol	units
Electron spectrum		
–primary	$dN_e/dE_e \propto E_e^{-\alpha_e^{\text{prim}}}$	$\text{GeV}^{-1}\text{s}^{-1}\text{sr}^{-1}\text{cm}^{-2}$
–secondary	$dN_e/dE_e \propto E_e^{-\alpha_e^{\text{sec}}}$	$\text{GeV}^{-1}\text{s}^{-1}\text{sr}^{-1}\text{cm}^{-2}$
Electron energy	E_e	keV
e spectral index		
– primary	α_e^{prim}	
– secondary	α_e^{sec}	
Proton spectrum		
	$dN_p/dE_p = A_p \cdot (E_p/E_{\text{max}})^{-\alpha_p} \cdot \exp(-E_p/E_{\text{max}})$	$\text{GeV}^{-1}\text{s}^{-1}\text{sr}^{-1}\text{cm}^{-2}$
Proton energy	E_p	GeV
p spectral index	α_p	
p cutoff energy	E_{max}	GeV
Neutrino spectrum		
Neutrino energy	E_ν	GeV
ν spectral index	α_ν	
normalization factor	A_ν	$\text{GeV}^{-1}\text{s}^{-1}\text{sr}^{-1}\text{cm}^{-2}$
Radio flux density		
– at 1.4 GHz, 2.4 GHz, 2.7 GHz & 5 GHz	$S_{1.4\text{GHz}}, S_{2.4\text{GHz}}, S_{2.7\text{GHz}}, S_{5\text{GHz}}$	mJy
IR flux density, IRAS		
– at $12\mu\text{m}$, $25\mu\text{m}$, $60\mu\text{m}$ & $100\mu\text{m}$	$S_{12\mu}, S_{25\mu}, S_{60\mu}$ & $S_{100\mu}$	Jy
IR flux density, 2MASS		
– at $1.25\mu\text{m}$, $1.65\mu\text{m}$ & $2.17\mu\text{m}$	$S_{1.25\mu\text{m}}, S_{1.65\mu\text{m}}, S_{2.17\mu\text{m}}$	Jy
X-ray flux density, ROSAT		
–btw. [0.1-4.5],[0.1-2.3] or [0.2-2.0] keV	S_{ROSAT}	nJy
spectral index		
– btw 1.4 GHz & 5 GHz	α	
– btw 1.4 GHz & $60\mu\text{m}$	α_{fir}	
– btw $60\mu\text{m}$ & $\sim 1\text{keV}$	α_{xir}	

Table 1. Summary of parameters used in this paper.

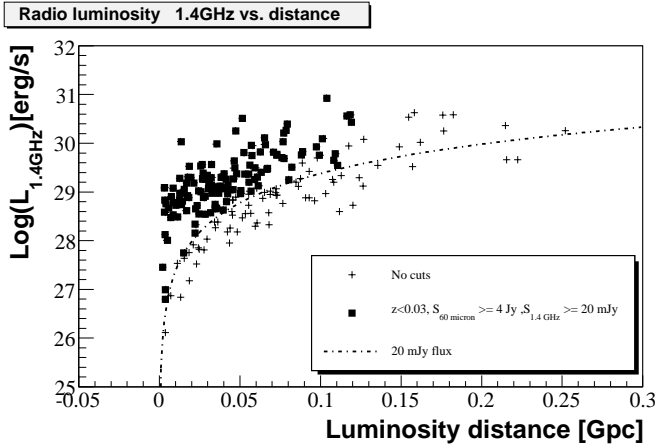


Fig. 2. 1.4 GHz luminosity - distance diagram. Same notation as Fig. 1. The dashed line shows the sensitivity for $S_{1.4\text{GHz}} > 20\text{ mJy}$.

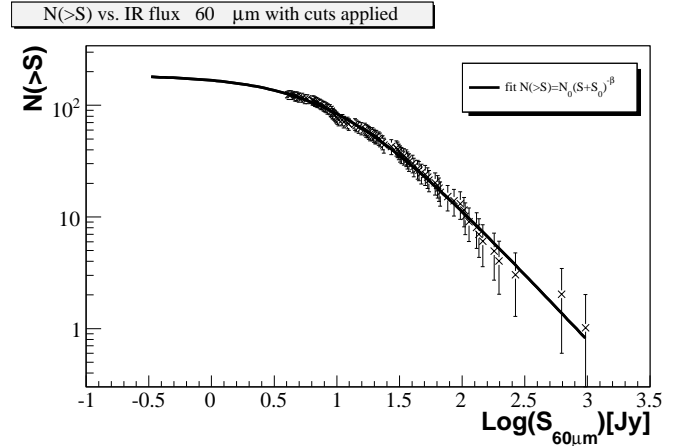


Fig. 3. $\log N - \log S$ representation of the catalog. An $S^{-1.2}$ -fit matches the data nicely, with a turnover at $S_0 = 10.56\text{ Jy}$.

flux density larger than S , $N(> S)$, should follow a behavior of $S^{-1} - S^{-1.5}$. A pure S^{-1} -behavior is expected for a flat cylinder, while a spherical distribution results in an $S^{-1.5}$ -behavior. Figure 3 shows the logarithmic number of sources above an FIR flux density $S_{60\mu}$. We fit the data with the following function:

$$N(> S) = N_0 \cdot (S + S_0)^{-\beta} \quad (2)$$

Here, N_0 , S_0 and β are fit parameters. Using an error of \sqrt{N} , the parameters are determined to

$$\begin{aligned} N_0 &= 3155 \pm 1297.9 \\ S_0 &= (10.56 \pm 3.78)\text{ Jy} \\ \beta &= 1.2 \pm 0.2. \end{aligned}$$

The behavior $N(> S) \sim S^{-1.2 \pm 0.2}$ matches the expectation that the function should lie between $S^{-1.0}$ and $S^{-1.5}$. In the following paragraphs, we will investigate further whether the classification of the 127 sources as starbursts is justified.

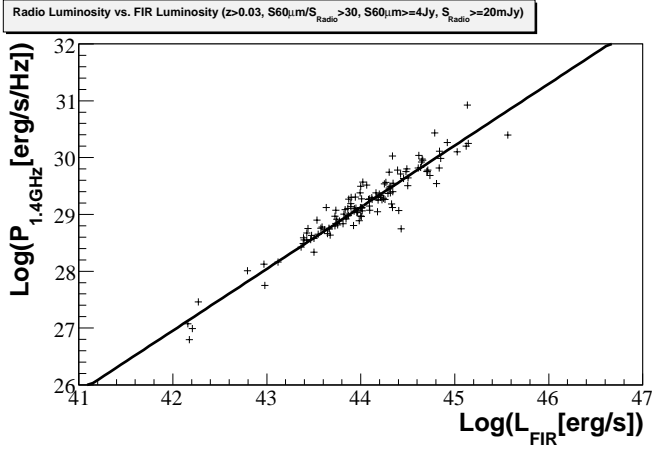


Fig. 4. Radio power $P_{1.4\text{GHz}}$ at $\nu = 1.4$ GHz versus FIR luminosity L_{FIR} . A direct proportionality, $P_{1.4\text{GHz}} \propto L_{\text{FIR}}$ is found.

3.1. FIR luminosity versus Radio power

Looking at a well defined sample of galaxies, it turns out that the correlation between radio and far-infrared (FIR) emission is *not* linear, i.e., that the radio luminosity is proportional to the far-infrared luminosity to the power 1.30 ± 0.03 (Xu et al., 1994b). As Xu and collaborators note, the far-infrared emission has two heating sources, stars that do explode later as supernova remnants, and also stars, that will never explode as supernovae. This second population of stars needs to be corrected for, and their contribution to the dust heating needs to be eliminated. This then leads to a corrected far-infrared luminosity, which is directly proportional to the radio luminosity (Xu et al., 1994b). The proportionality holds along a disk in a galaxy, even for fairly short lived phases like a starburst, such as in M 82, and thus requires clearly local physics, with a short readjustment time scale. This poses a severe difficulty for any proposal to explain the radio/FIR correlation.

The FIR luminosity in the range of $60\mu\text{m}$ and $100\mu\text{m}$ is given as (Xu et al., 1994b):

$$L_{\text{FIR}} := 4\pi d_l^2 \cdot F_{\text{FIR}}. \quad (3)$$

Here, d_l is the luminosity distance of the individual sources and

$$F_{\text{FIR}} := 1.26 \cdot 10^{-14} \cdot \left[2.58 \cdot \left(\frac{S_{60\mu}}{\text{Jy}} \right) + \left(\frac{S_{100\mu}}{\text{Jy}} \right) \right] \text{W m}^{-2} \quad (4)$$

is the FIR flux density at Earth as defined in Helou et al. (1988). The normalization factor comes from the frequency integration and from the conversion of Jy to $\text{W/m}^2/\text{Hz}$. In Fig. 4, the logarithm of the radio power at 1.4 GHz, $P_{1.4\text{GHz}}$ versus the logarithm of the FIR luminosity L_{FIR} is shown for our catalog. The circles show the single sources and the solid line is a fit through the data. The fit yields a correlation of

$$P_{1.4\text{GHz}} \propto L_{\text{FIR}}^{1.0}. \quad (5)$$

This demonstrates that short stellar lifetimes dominate the correlation in our sample, and so this is strongly supporting our hypothesis, that the majority of our sample galaxies are starbursts.

3.2. Infrared to radio flux density ratio

Generally, regular galaxies are distinguished from active galaxies by their ratio of the FIR flux density at $60\mu\text{m}$, $S_{60\mu}$, and the

radio flux density at 1.4 GHz, $S_{1.4\text{GHz}}$:

$$s_{60\mu/1.4\text{GHz}} := \frac{S_{60\mu}}{S_{1.4\text{GHz}}}. \quad (6)$$

For Seyfert galaxies, this ratio is about $s_{60\mu/1.4\text{GHz}} \sim 10$, while it is significantly higher in the case of starburst galaxies, $s_{60\mu/1.4\text{GHz}} \sim 300$. The histogram of the ratio between the FIR flux density at $60\mu\text{m}$ and the radio flux density at 1.4 GHz is shown in Fig. 5. All 127 sources have a ratio of $s_{60\mu/1.4\text{GHz}} > 30$, which confirms that the sources are not likely to be Seyferts.

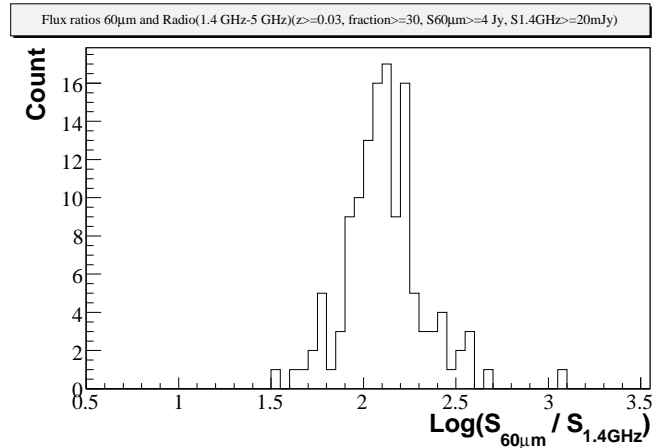


Fig. 5. Ratio of the flux density at $60\mu\text{m}$ and at 1.4 GHz. All sources in the sample have ratios larger than 30, which indicates a high star formation rate. The median is around 100. This matches previous investigations, e.g. Biermann et al. (1985), who find a mean value of 250 at higher radio frequencies, $\nu = 5$ GHz.

3.3. Radio to Infrared and X-ray to Infrared spectral indices

A further criterion of distinguishing regular galaxies and Seyferts is their spectral index from X-ray to IR (XIR) and from radio to IR (RIR). The diagram of the XIR (1 keV to $60\mu\text{m}$) versus RIR (5 GHz to $60\mu\text{m}$) index of the sources in shown in Fig. 6. Derived from figure 3 in (Rodríguez-Pascual et al., 1993), starburst galaxies have spectral indices scattering around $(\text{RIR}, \text{XIR})_{\text{starburst}} \sim (0.6, -1.9)$, Seyfert-I galaxies show $(\text{RIR}, \text{XIR})_{\text{Seyfert-I}} \sim (0.48, -1.2)$, Seyfert-II galaxies have $(\text{RIR}, \text{XIR})_{\text{Seyfert-II}} \sim (0.47, -1.6)$ and quasars are located at $(\text{RIR}, \text{XIR})_{\text{quasar}} \sim (0.28, -1.1)$. The values for the RIR and XIR indices of starburst galaxies given by Chini et al. (1989) are slightly higher, which matches the sample examined here: Chini et al. (1989) give a RIR index of 0.82 and a XIR index of -1.66 . We find average values of $(\overline{\text{RIR}}, \overline{\text{XIR}}) = (0.82, -1.77)$ which is compatible with the expected result.

Still, we do not have X-ray data for all the sources, so there may still be some contamination from both Seyferts and regular galaxies in the sample. As we only used catalogs where the sources have previously been identified as starbursts, this contamination should be small.

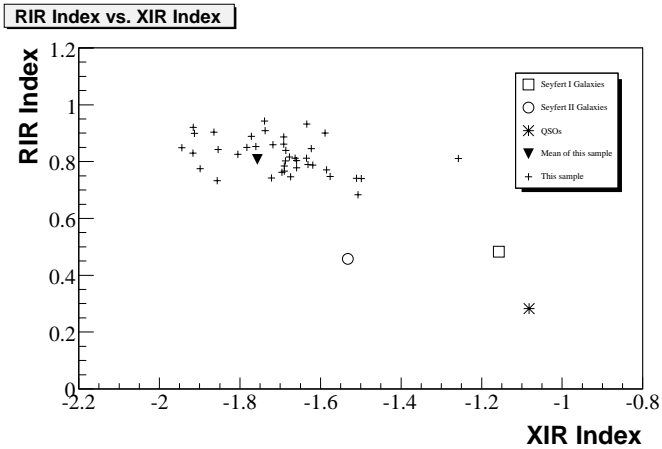


Fig. 6. Radio-to-IR spectral index versus X-ray-to-IR spectral index. The crosses represent those 48 sources in our catalog with radio, FIR and X-ray measurements. The blue triangle shows the average of the values. The open circle shows the average location of Seyfert-I galaxies, the open square represents average Seyfert-II galaxies and the star indicates QSOs. The last three values are taken from Rodriguez-Pascual et al. (1993). Note that individual galaxies scatter around the given values (Chini et al., 1989).

4. The interstellar medium and the FIR/radio correlation

The interstellar medium connects the formation of stars, the explosion of supernova remnants, the regularization and enhancement of the magnetic field, and the transport of cosmic rays. In order to understand the observation that the thermal hot dust emission from a galaxy is simply proportional to the non-thermal radio emission from relativistic cosmic ray electrons, we need to understand the interstellar medium, or at least get close enough to a comprehension, that we can understand this amazing correlation (de Jong et al., 1985; Wunderlich et al., 1987; Wunderlich & Klein, 1988, 1991; Condon et al., 1991). Obviously, since the very massive stars power the far-infrared emission through a large fraction of the ultra-violet emission, which is absorbed by dust, and then in supernova explosions produce the energetic cosmic ray electrons, which emit the observed radio emission, there should be a correlation. Using simple initial models for stellar population evolution, this rather naive early picture successfully predicted the approximate far-infrared emission already in 1977 (Biermann, 1976; Biermann & Fricke, 1977; Kronberg & Biermann, 1981). However, the tightness of the correlation was neither anticipated nor predicted. The correlation was finally discovered by de Jong et al. (1985). Since the dust emission just measures the total output in ultra-violet by young stars, it seems obvious, that in the limit of much absorption, the far-infrared emission would just be proportional to the star formation rate, given a general initial mass function. However, the radio emission is approximately proportional to the product of the cosmic ray electron density and the magnetic field energy density, and therefore it is not really obvious at all, that integrating along a vertical column through the disk of a galaxy these two emission components should be basically proportional.

Modern descriptions of starburst galaxies such as M 82 or NGC 2146 are in Dopita et al. (2005, 2006a,b); Groves et al. (2008).

It had been observed early that the three main components of the interstellar medium, the gas, the cosmic rays, and the magnetic field have very similar energy densities, or pressures. Since all three derive from very different physical processes, to keep them at approximate equipartition implies that the three time scales of change are also all three the same. This is the basic premise of the following argument, and it will lead naturally to an understanding of the far-infrared radio correlation. So in this specific sense it is a calorimetric argument similar to Völk (1989), although we approach the problem in a somewhat different way.

The following line of reasoning is visibly influenced by earlier papers, like Biermann (1950); Biermann & Schlüter (1951); Cox (1972); Cox & Smith (1974); McKee & Ostriker (1977); Beuermann et al. (1985); Kronberg et al. (1985); Kronberg & Sramek (1985); Snowden et al. (1997); Hunter et al. (1997); Beck et al. (2003); Hanasz et al. (2004, 2006), and of course others mentioned in due course.

First we wish to establish the concepts which we use, for easy reference, and then apply them to the problem here.

4.1. The three main components of the interstellar medium

The three main components are the gas, the cosmic rays and the magnetic field. At least the gas and the magnetic field is clearly spatially highly inhomogeneous (Beck et al., 2003):

The gas has a number of components, molecular clouds, neutral Hydrogen clouds, diffuse neutral Hydrogen, diffuse ionized Hydrogen, HII regions, stellar wind bubbles, supernova remnants with X-ray emitting shells, a tunnel network of connected older supernova remnants (Cox & Smith, 1974), a thick hot disk (Beuermann et al., 1985; Snowden et al., 1997; Kronberg et al., 2007), and a wind (Breitschwerdt, 2008; Everett et al., 2008). The tunnel network probably connects to the hot thick disk. The wind is probably fed from the hottest regions of the tunnel network, in a fashion perhaps similar to the Solar wind being fed from coronal holes (Stepanian et al., 2008, e.g.).

The magnetic field is permeating almost everything, and also has a thick disk. The field permeates the clouds, and is often confined visibly by the clouds (Appenzeller, 1974, e.g.). The magnetic field is strongly perturbed by HII regions, and supernova explosions. The magnetic field is transported out of the disk by the wind.

The cosmic rays, produced by supernova explosions in shockwaves (Baade & Zwicky, 1934; Fermi, 1949; Drury, 1983; Berezhinsky et al., 1990) cannot easily be repelled by anything, and so go through all clouds, and all the neutral and ionized gas. In bulk they cannot travel faster than the Alfvén speed, since otherwise they would excite waves in the plasma, scattering the particles, effectively reducing their bulk velocity.

The magnetic field is instrumental to allow cosmic ray acceleration in shocks, and perhaps throughout the medium.

The cosmic rays in turn drive the dynamo mechanism to enhance an existing magnetic field and give it spatial coherence (Parker, 1969, 1992; Ferrière, 1996; Ferrière & Schmitt, 2000; Hanasz et al., 2004, 2006; Otmianowska-Mazur et al., 2008). In the classical Biermann-battery mechanism (Biermann, 1950; Biermann & Schlüter, 1951), only a rotating star with surfaces of density and pressure in non-coincidence is required to produce a seed field, which, however, is generally weak; the dynamo mechanism in stars can strongly enhance magnetic fields, and through winds eject them (Bisnovatyi-Kogan et al., 1973, e.g.): This would constitute a very irregular, but potentially relatively strong source of magnetic fields in galaxies; in such a case the dynamo mechanism on a Galactic scale is required more to reg-

ularize the field rather than to strengthen it. In the mechanism of Lucek & Bell (2000); Bell (2004, 2005) the shock waves can directly enhance the magnetic field, using an existing population of cosmic rays. As noted already, the cosmic rays couple effectively to the gas. Anisotropies in the phase space distribution of particles, always present in shockwaves, also can produce new magnetic fields on small scales (Weibel, 1959; Bykov & Toptygin, 2005). Galactic magnetic fields have also been reviewed by Beck et al. (1996); Kulsrud (1999); Kulsrud & Zweibel (2008).

Thermodynamically both the cosmic rays and the magnetic field can be thought of as a relativistic gas, with almost zero net mass density.

Therefore the ensemble of cosmic rays and magnetic field constitute a light fluid pushing against the heavy fluid of the normal gas, and given enough energy density, these two components escape via an instability (Parker, 1965; Kowal et al., 2003, 2006).

Therefore all three components are strongly coupled, and the data confirm an approximate energy equipartition between cosmic rays and the magnetic field, and the sum of these two components equal in energy density to the gas.

The one given parameter is the total energy input, integrated across all spatial inhomogeneities, since the energy supply is given by the stars, in the form of winds, explosions, and radiation. Since the inhomogeneities are extreme, especially in the density, it is important to use spatially integrated energy densities for reference as much as possible. So we note that the energy density of the magnetic irregularities integrated over all spatial scales is also in approximate equipartition (Beck et al., 1996).

The energy input can be estimated from the explosions of supernovae to about 1 supernova of 10^{51} erg, every 100 years, so at $L_{kin} = 3 \cdot 10^{41}$ erg/s; the uncertainty in this is about a factor of 3. Some fraction of this energy goes into cosmic rays. This fraction could be large (Drury, 1983).

Other energy input can be estimated from the infrared emission (Cox & Mezger, 1989): About 1/3 to 1/4 of the total stellar radiation is absorbed by dust and reradiated in the infrared, beyond a wavelength of 25μ , about $10^{10} L_{\odot}$. Of this, about $2 \cdot 10^9 L_{\odot} = 8 \cdot 10^{42}$ erg/s is coming from young star forming regions.

The energy density of magnetic fields can be estimated to be about $1.6 \cdot 10^{-12}$ dyn/cm² (Beck et al., 1996; Everett et al., 2008), the energy density of cosmic rays is about the same, and their sum is about equal to the gas pressure, of $4 \cdot 10^{-12}$ dyn/cm². Using a scale height of full width of 3 kpc, and a radius of 10 kpc, we obtain a crude estimate of the energy content. This requires for magnetic fields and cosmic rays together an average supply of energy of about $4 \cdot 10^{41}$ erg/s, using the time scale obtained from cosmic rays (see below). Such numbers are uncertain by probably a factor of 2. Everett et al. (2008) also estimate the required wind-power to about $4 \cdot 10^{41}$ erg/s, a Galactic wind driven by cosmic rays; they discuss other estimates.

It is interesting to note that to within the uncertainties all these power estimates (supernovae, wind power, magnetic field and cosmic ray replenishment) agree better than their respective error estimates.

Therefore the time scales to replenish anyone of the components must also be approximately be the same. We do have the real number from radioactive isotopes of cosmic rays interacting, and the number is about 10 million years (Brunetti & Codino, 2000, e.g.). This is then the time scale for all key processes.

4.2. Supernova explosions

For didactic simplicity we basically adopt the approach of Sedov (1958); Cox (1972), but use more modern cooling approximations, and allow for much lower environmental densities, but otherwise rescale their equations.

An explosion runs into the interstellar medium, and expands into the tenuous gas, which surrounds the clouds, and extends far above and below the central layer of cool clouds. We consider the expansion into the surrounding low density medium and ask, when the expansion runs into the cooling limit:

The first question is what density should be used: The galaxy has a wind (Westmeier et al., 2005; Breitschwerdt, 2008; Everett et al., 2008; Gressel et al., 2008; Otmianowska-Mazur et al., 2008) and it is getting fed from the tunnel network of Cox & Smith (1974) probably. This implies that the Alfvén speed must approach the escape speed, for a cosmic ray driven magnetic wind. Other galaxies also show evidence for winds (Chyży et al., 2000a,b; Chyży & Beck, 2004; Chyży et al., 2006, 2007):

$$V_A = \frac{B}{4\pi\rho} \approx 400 \text{ km/s.} \quad (7)$$

With $B \approx 3 \mu\text{Gauss}$, this implies a density of about $n = 3 \cdot 10^{-4} \text{ cm}^{-3}$.

The time to start cooling is

$$\tau^c = 5 \cdot 10^6 \text{ yrs} \left(\frac{E_{51}}{n_{-3.5}} \right)^{2/11} (r\Lambda_{-21} n_{-3.5})^{-5/11}, \quad (8)$$

where E_{51} is the energy of the explosion in units of 10^{51} erg, $n_{-3.5}$ is the tenuous density in units of $3 \cdot 10^{-4} \text{ cm}^{-3}$, Λ_{-21} is the cooling coefficient in units of $10^{-21} \text{ erg cm}^3 \text{ s}^{-1}$, and r is a compaction parameter of order unity. This low density reflects the finding that the tenuous medium is of very low density, and due to substructure may on volume average be of even lower density than suggested by the X-ray data (Snowden et al., 1997; Everett et al., 2008), of order $3 \cdot 10^{-3} \text{ cm}^{-3}$; but we do use the temperature of 10^5 K, near the maximum, and also close to the stable region (Field, 1965). However, the cooling suggested by the X-ray spectrum is an integral over the entire evolution, and so only sensitive to the earliest part of the evolution. As soon as two or more supernova remnants overlap, and start building a network (Cox & Smith, 1974), then the temperature evolution will be different, giving again higher temperatures, consistent with observations.

The radius at that stage is

$$R^c = 8 \cdot 10^2 \text{ pc} \left(\frac{E_{51}}{n_{-3.5}} \right)^{3/11} (r\Lambda_{-21} n_{-3.5})^{-2/11} \quad (9)$$

and the temperature then is initially

$$T^d = 1.7 \cdot 10^5 \text{ K} \left(\frac{E_{51}}{n_{-3.5}} \right)^{2/11} (r\Lambda_{-21} n_{-3.5})^{6/11}. \quad (10)$$

This corresponds to an injection scale of turbulence. Interestingly, the time scale is of the same order of magnitude to what we derive from cosmic ray transport, and the length scale is not far from the scale height of the hot disk (Snowden et al., 1997), demonstrating qualitative consistency. We note that Snowden et al. (1997) gave a much higher temperature, of about $4 \cdot 10^6$ K, with a density of $3 \cdot 10^{-3} \text{ cm}^{-3}$. Also, Everett et al. (2008) suggest a higher temperature. However, the

luminosity of that phase is a very small fraction of the entire dissipation in the ISM.

As Field (1965) shows the cooling is stable if the temperature dependence of the cooling function Λ is sufficiently strong and its double logarithmic derivative positive, or in the presence of heating larger than 2. This is the cooling phase we are interested in. This is the case at temperatures below and near about $\sim 10^5$ K.

Data suggest that the break-up of supernova remnant shells has been observed in the starburst galaxy M82 (Bartel et al., 1987). However, in that case it is not clear whether we are observing the break-up of a wind-shell produced in a snow-plow effect by the stellar wind prior to the supernova explosion, or the break-up of the snow-plow of the normal supernova exploding into the interstellar medium.

4.3. Magnetic inhomogeneities

In the magnetic field data in our galaxy (Beck et al., 2003) there is already strong evidence for small scale substructure, since different measures of the magnetic field yield very different numbers: linear measures such as Faraday Rotation Measures indicate much lower strengths of the magnetic field than quadratic measures such as synchrotron emission. This is typical for small scale substructure (Lee et al., 2003; de Avillez & Breitschwerdt, 2004, 2007), where for a given total energy content high intensity sheets can hold all the energy for a small volume fraction. In such a picture linear measures give a much smaller number than quadratic measures, as is well known from mathematically isomorphic arguments in thermal emission. Of course we should be comparing the proper integrals, also involving the spatial distribution of thermal electron density and cosmic ray electron density (see, e.g., Bowyer et al. (1995)). We ignore all this in our simple exercise.

We can quantify this by integrating along a long thin cylinder of unit length. We refer to the magnetic field as B_0 , when it is homogeneous, and for the inhomogeneous case the magnetic field is B_1 over most of the length, and enhanced by a factor $1/x$ in a region of length x : This then gives for the integrated energy density

$$B_1^2 \cdot \frac{1}{x} + B_1^2 \cdot (1-x) = B_0^2. \quad (11)$$

Keeping the integrated energy content B_0^2 constant, the linear measure of the magnetic field is given by

$$B_1 \cdot \frac{1}{x} \cdot x + B_1 \cdot (1-x) = B_1 \cdot (2-x). \quad (12)$$

Combining the two expressions gives

$$\sqrt{\frac{x}{1-x}} \cdot (2-x) \quad (13)$$

for the ratio of linear measure versus quadratic measure. In the limit of small x this is just \sqrt{x} . The observations suggest that this ratio is of order 1/5 (Beck et al., 2003), and so $x = 0.04$ by order of magnitude. This implies that most of the magnetic energy is contained in shells of a volume a few percent, possibly as low as 1 percent. Since the linear measure is proportional to the bending of ultra high energy cosmic rays, this implies that the bending is reduced by a factor between 5 and 10 over what we might reasonably expect otherwise. Obviously, in realistic situations much of this effect will be smoothed out, and so perhaps even more extreme situations may be required.

Using the approach of Cox (1972) with the environment of the tenuous hot phase of the interstellar medium (Snowden et al., 1997; Everett et al., 2008) the cooling stage of an expanding shell of a supernova remnant might lead to such a configuration, of a very thin shell at large distances, with strong magnetic fields. In such a picture this stage would encompass most of the supernova's energy dissipation, and so similar considerations may apply to the interpretation of the X-ray data (Snowden et al., 1997; Everett et al., 2008).

4.4. Turbulence

Turbulence is an ubiquitous phenomenon, and also is a key ingredient in the interstellar medium (see reviews by Rickett (1977); Goldstein et al. (1995)). Key concepts to turbulence theory have been introduced by Prandtl (1925); Karman & Howarth (1938); Kolmogorov (1941a,b,c); Obukhov (1941); Heisenberg (1948); Kraichnan (1965), and have been reviewed by Sagdeev (1979). One key argument which we wish to use, is the concept of the turbulent cascade. There the energy of the turbulence is injected into the gas at some large wavelength, and cascades down through wavenumber space, to the small wavelengths where the energy is dissipated. In many examples this leads in a three-dimensional isotropic model to the Kolmogorov cascade, which can be described in a local approximation by the following diffusion equation in wavenumber space (McIvor, 1977; Achterberg, 1979):

$$\frac{d}{dt} \frac{I(k)}{4\pi k^2} - \frac{1}{k^2} \frac{\partial}{\partial k} \left(\frac{k^4}{3\tau_k} \frac{\partial}{\partial k} \left(\frac{I(k)}{4\pi k^2} \right) \right) = A \delta(k - k_o) \quad (14)$$

Here $I(k)$ is the energy density of the turbulence per wavenumber k , and per volume element, and τ_k is the time scale of diffusion, which can be written as

$$\tau_k = \frac{1}{k(\gamma_{eff} I(k) k / \rho)^{1/2}}. \quad (15)$$

Here ρ is the matter density, and γ_{eff} is an effective adiabatic constant for the turbulent energy. The turbulence has a source-term, here limited to a single wavenumber k_o . The turbulence diffusion equation basically says that the turbulence moves through wavenumber space with no additional source or sink, as a constant energy current in wavenumber phase space (Kolmogorov, 1941a,b,c). The solutions to this diffusion equation can be written as

$$\begin{aligned} I(k) &\sim k^2 \quad \text{for } k \leq k_o \text{ and} \\ I(k) &\sim k^{-5/3} \quad \text{for } k \geq k_o. \end{aligned} \quad (16)$$

This latter behavior is commonly referred to as the Kolmogorov cascade, and is found ubiquitously in nature.

4.5. The cooling of the interstellar medium

The interstellar medium has a number of phases, which appear to be in approximate pressure equilibrium. Concentrating on the phase of the highest temperature, the highest speed of signalling (be it sound waves, or Alfvén waves, or other wave modes), we note that its temperature is in the range where the typical gaseous emission is detected in the X-ray regime. The cooling curve of such a gas has been extensively discussed by many (Cox, 1972;

Sutherland & Dopita, 1993; Dopita & Sutherland, 2003, e.g.). It shows the following features, starting at low temperature, and considering the cooling coefficient $\Lambda(T)$ with n the interstellar density in particles cm^{-3}

$$n^2 \Lambda(T) \text{ erg/cm}^3/\text{sec}. \quad (17)$$

This cooling curve $\Lambda(T)$ rises from near 10^4 K to a local peak near $\approx 3 \cdot 10^5$ K. The level of cooling along this local peak is given by $\Lambda \approx 10^{-21}$ ergs/cm³/s, dropping to $\Lambda \approx 10^{-22}$ ergs/cm³/s near $\approx 10^6$ K, and towards a minimum near $\Lambda \approx 3 \cdot 10^{-23}$ erg/cm³/s in the range $\approx 3 \cdot 10^6$ K to $\approx 10^8$ K. The peak is due to many edges and lines in the soft X-ray range. At higher temperatures the continuum emission begins to dominate and that emission is then given by $\Lambda \approx 1.4 \cdot 10^{-27} T^{1/2}$ erg/cm³/s. The sharp cutoff to low temperatures near 10^4 K is due to beginning recombination and thus a smaller density of free electrons to interact with. A contemporary discussion including the effects of strong departures from ionization equilibrium has been given by Schmutzler & Tscharnuter (1993); Breitschwerdt & Schmutzler (1994).

4.6. The leaky box approximation

Consider a column perpendicular to a galactic disk of height H , and the number of cosmic ray particles in it as a function of particle energy and time $N(E, t)$; then we have the balance equation

$$\frac{d}{dt}N(E, t) + \frac{N(E, t)}{\tau(E)} = Q(E). \quad (18)$$

where $\tau(E)$ is the escape time scale. The sign of the second term is positive, since the process described is a loss. In a stationary state we then obtain readily

$$N(E) = Q(E) \tau(E). \quad (19)$$

The characteristic time of loss can be written as

$$\tau(E) \sim \frac{H^2}{\kappa}. \quad (20)$$

Here, κ is the diffusion coefficient of cosmic ray particles, which can be written approximately in the quasi-linear approximation as

$$\kappa \sim \frac{1}{3} r_g c \frac{B^2/8\pi}{I(k)k}, \quad (21)$$

where we write for the turbulent energy density

$$I(k)k \sim I_0 k_0 (k/k_0)^{-2/3} \sim I_0 k_0 B^{-2/3} r_0^{-2/3} E^{2/3}, \quad (22)$$

using here the assumption of a Kolmogorov spectrum. Here, $r_g \sim 1/k \sim E/B$ is the Larmor radius of a particle of energy E under consideration, which gyrates in a magnetic field of strength B . The basic radius $r_0 \sim 1/k_0$ corresponds to the injection scale of the turbulence. This then leads to a dependence of the diffusion coefficient on the various parameters

$$\kappa \sim E^{1/3} B^{5/3} r_0^{2/3} I_0^{-1} k_0^{-1}. \quad (23)$$

Therefore, we adopt the point of view that the leakage time scale $\tau(E)$ is proportional to (relativistic) energy $E^{-1/3}$, and so that the equilibrium density of energetic particles $N(E)$ is proportional to $E^{-1/3}$ as well.

There is a difficulty with this argument, which can be solved: The secondary to primary ratio of cosmic ray nuclei such as

the ratio Boron to Carbon already give information as to the energy dependence of the leakage time, and such an analysis gives an energy dependence as $E^{-0.6 \pm 0.1}$ (Engelmann et al., 1990, e.g). We have argued elsewhere already (Biermann, 1995; Wiebel-Sooth et al., 1995, 1998), that this reflects the energy dependence of the amount of target material seen for spallation. Most of the target interaction with heavy nuclei among the cosmic rays happens near the most massive stars, the Wolf-Rayet stars, with the turbulence excited by the cosmic rays themselves, giving an energy dependence of the spallation secondaries of $E^{-5/9}$ (Biermann, 1998; Biermann et al., 2001; Biermann, 2006), consistent with the data, which give $E^{-0.54}$ (Ptuskin, 1999). On the other hand, most of the gamma emission from π -zero decay arises from the interaction among the more numerous supergiant stars, the red supergiants, for which we suggest that the turbulence arises from instabilities.

4.7. The radio emission

In order to calculate the radio emission from the total number of relativistic electrons in a column we first have to proceed to work out the cosmic ray loss time for electrons, second the cooling time for the tenuous hot medium, put them equal, and third calculate the radio emission per supernova event from a column in the disk.

The maximum energy in the elemental distribution and spectrum of the cosmic rays is in protons near their rest mass energy, since their spectrum is steeper than 2 in energy. This means that the energy which has to be used in the expression for the leakage time is fixed. So, the leakage time is given by

$$\tau_{CR} \sim \frac{H^2 I_0 k_0}{B^{5/3} r_0^{2/3} E^{1/3}}. \quad (24)$$

The maximum energy content of the population in the proton spectrum is here near $E = 1$ GeV, so that

$$\tau_{CR}(E = 1 \text{ GeV}) \sim \frac{H^2 I_0 k_0}{B^{5/3} r_0^{2/3}}. \quad (25)$$

in this case.

The cooling time is given by

$$\begin{aligned} \tau_{cool} &\sim \frac{nk_B T}{n^2 \Lambda(T)} \sim \frac{B^2/8\pi}{(B^2/8\pi/2k_B T_\star)^2} \frac{1}{\Lambda(T_\star)} \\ &\sim \frac{T_\star^2}{\Lambda(T_\star)} \frac{1}{B^2} \sim \frac{1}{B^2} \end{aligned} \quad (26)$$

in the approximation that $\Lambda(T_\star)/T_\star^2$ is a constant, and assuming equipartition again. This is reasonable in the dissipation stage of supernova remnants when Λ approaches a double-logarithmic derivative of 2, below a temperature of 10^5 K. Also, in that temperature range the cooling time is a minimum, for a given energy density. We noted above that the dissipation stage reaches those temperatures.

Putting the two time scales equal then yields the relation

$$\frac{H^2 I_0 k_0}{B^{5/3} r_0^{2/3}} \sim \frac{1}{B^2}. \quad (27)$$

Now, we wish to consider electrons, which emit radio emission at a certain frequency ν , which gives the condition that

$$E \sim \nu^{1/2} B^{-1/2} \quad (28)$$

and so, making use of the frequency and magnetic field dependence of Equ. (26) and Equ. (28), the diffusion time for electrons which emit at ν is given by

$$\tau_{CR,e} \sim H^2 E^{-1/3} B^{-5/3} r_o^{-2/3} I_o k_o \sim B^{-11/6} \nu^{-1/6} \quad (29)$$

The emission is from a spectrum of electrons of $E^{-2.42 \pm 0.04}$ at injection (Biermann & Strom, 1993), and so the total radio emission S_ν per supernova event in a column in a disk can be written as

$$\begin{aligned} S_\nu &\sim B^{1.71 \pm 0.02} E_{SN,CR,e} \nu^{-0.71 \pm 0.02} B^{-11/6} \nu^{-1/6} \\ &\sim B^{-0.12 \pm 0.02} \nu^{-0.88 \pm 0.02} \end{aligned} \quad (30)$$

for the case that all supernova remnants produce the same number of relativistic electrons. Here, we use an integration along a vertical column to obtain the total number of energetic electrons per supernova explosion. This is reasonable since we are using the adiabatic phase of supernova remnant evolution, where the energy is conserved. This argument leads to such a weak dependence on the strength of the magnetic field, that the resulting offset is smaller than the errors in the data.

Therefore the radio emission is only very weakly dependent on the magnetic field, independent of all other parameters, and is directly proportional to the number of supernovae per time interval, and so also to the luminosity of massive stars.

The cosmic ray electron data show that above a few 10 of GeV the spectrum is already in the loss limit, so steeper by unity (Kardashev, 1962). Below that energy the direct data are compromised by the Solar wind modulation, but from the radio emission of normal galaxies we do know that the electron spectrum is closely in agreement with what we obtain for protons, at somewhat higher energy, allowing us to conclude that the electron spectrum corresponds to the diffusion limit, when the leakage out of the Galaxy is faster than the synchrotron loss. Using the expressions for the two time scales we can check:

Radio emission at 5 GHz corresponds to an electron energy of 8 GeV, and a synchrotron loss time of $4 \cdot 10^7$ yr.

As we note elsewhere, galaxies and starburst galaxies are sometimes so young as to be in the injection limit, or so old as to be in the loss limit, rather than the leakage or diffusion limit that we consider here. For any reasonably young age of a starburst there is always some low radio frequency ν_1 , below which we are still in the injection stage, below which the age of the starburst is longer than the diffusion time scale. So below that the radio flux density is lower than the diffusion limit derived above, and the radio flux density has the spectrum of injection, following Biermann & Strom (1993) $S_\nu \sim \nu^{-0.71}$, and so relative to the diffusion limit the radio emission at frequency $\nu < \nu_1$ is weaker by the factor $(\nu/\nu_1)^{1/6}$; this is typically not far below unity. At the other extreme, considered by Völk (1989) there is also a radio frequency ν_2 , beyond which the synchrotron and inverse Compton losses cut in, and become faster than the diffusion. This is directly visible in the observed cosmic ray electron spectra (Wiebel-Sooth & Biermann, 1999). So, at radio frequencies $\nu > \nu_2$ the radio emission is again weaker, this time by $(\nu/\nu_2)^{-1/3}$. So again the radio emission is slightly down. Both variants show, that the radio emission is not far from the diffusive equilibrium. This concludes the demonstration of the argument. There are many checks on these ideas, which one can make, such as the pressure of the interstellar medium, the X-ray luminosity, the possibility to account for extreme galaxies such as M82, the radial gradient of the far-infrared/radio ratio (Bicay et al., 1989), the thickness of the hot gaseous disk and the associated diffusion coefficient of cosmic rays, and many others. We will discuss these points elsewhere.

4.8. Where is the limit to the diffusion limit?

The line of reasoning seems to be a deus ex machina in the sense that we seem to be always in the diffusion limit, independent of whether we have starburst galaxies with relatively strong magnetic fields, or normal galaxies like our own.

The equations above imply that

$$\tau_{diff} = \frac{(2k_B T)^2 8\pi}{\Lambda B^2} < \frac{6\pi m_e c}{\sigma_T \gamma_e B^2} = \tau_{syn}. \quad (31)$$

We note first that both sides depend on the magnetic field strength squared, so the argument is independent on the magnetic field: Inserting numbers we find

$$\frac{(T_5)^2}{\Lambda_{-21}} < \frac{4 \cdot 10^7}{\gamma_e}, \quad (32)$$

where γ_e is the Lorentz factor of the mainly emitting electrons. This time, however, we need to ask what density contrast the main radio emitting substructures have, since the left hand side of the equation uses grand total volume averages, and the right hand samples just those regions, where B^2 is especially high. Already simple arguments, as shown above, demonstrate that the average of B^2 is quite a bit higher than the average of B squared. We can assume here, that such a factor might be of order 30, or even higher, bringing the limiting energy of the electrons down to $\gamma_e < 10^6$, or possibly even much less. We have already argued earlier that for the cooling to be maximal, the temperature has to be close to or below 10^5 K.

This allows us to understand perhaps, why galaxies are usually in the diffusion limit, sometimes of course, in a starburst, in the injection limit: In that case the overall spectrum corresponds to injection. There was just not enough time to achieve diffusive approximate equilibrium.

4.9. Implications

First of all, this theory does just what one would naively expect, relate the massive stars which heat the dust through their ultraviolet light directly with the subsequent supernovae. All the theory does, is work out the non-linearity inherent in synchrotron emission, and shows them to introduce negligible dependencies on various parameters.

Starburst galaxies as well as quiescent galaxies equally obey the correlation between the radio and the far-infrared emission. Therefore the theory implies by necessity that the magnetic field in a starburst region rises with the overall energy density.

Galaxies which are subject to substantial compression by an encounter with another galaxy, clearly have a magnetic field which is higher than corresponds to the energy density derived from star formation, and so may be expected to have more radio emission than indicated by the general radio-far-infrared correlation. This is borne out by at least one example (Hummel & Beck, 1995).

Furthermore, it is clear that for very short time scales, near order 10^7 years, the correlation cannot hold, since we then run into the lifetimes of the massive stars, which drive the energy balance in the interstellar medium.

There is likely also a lowest level of star formation activity, where the assumption that the hot medium is fully connected, fails. There one may expect also substantial departures from the correlation.

5. Cosmic rays and their secondaries

As stated above, the cosmic ray intensity from starburst galaxies scales with the radio and infrared emission of the sources. In this section, we discuss the emission scenarios for charged cosmic rays and hadronic interactions leading to high-energy photon and neutrino emission. There are two source classes within starbursts that can accelerate cosmic rays to high energies, namely shock fronts of supernova remnants and long Gamma Ray Bursts (GRBs), the latter being connected to supernova Ic explosions. In the first case, maximum energies are limited to less than 10^{15} eV and thus, the cosmic rays from starbursts cannot be observed directly due to the high cosmic ray background in our own Galaxy. Gamma Ray Bursts, on the other hand, were proposed as the origin of cosmic rays above the ankle, i.e. $E_{\text{CR}} > 3 \cdot 10^{18}$ eV, see Vietri (1995); Waxman (1995). Since a high star formation rate as it is present in starburst galaxies, leads to a high rate supernova explosions, an enhanced rate of long GRBs is expected. Thus, for closeby sources, the distribution of starburst galaxies can be used to test the hypothesis of cosmic rays from starbursts, as also discussed in Biermann et al. (2008).

The dominant source of secondary cosmic rays like high-energy photons and neutrinos is proton-proton interactions in dense hydrogen regions and proton-photon interactions in Gamma Ray Bursts. Proton-proton interactions produce pions via

$$pp \rightarrow \pi^+ \pi^- \pi^0. \quad (33)$$

Photohadronic interactions, on the other hand, yield pions via the Delta resonance,

$$p\gamma \rightarrow \Delta^+ \rightarrow n\pi^+ / p\pi^0. \quad (34)$$

High-energy photons and neutrinos are subsequently emitted in π^\pm - resp. π^0 -decays:

$$\begin{aligned} \pi^+ &\rightarrow \mu^+ \nu_\mu \rightarrow e^+ \nu_e \bar{\nu}_\mu \nu_\mu \\ \pi^- &\rightarrow \mu^- \bar{\nu}_\mu \rightarrow e^- \bar{\nu}_e \nu_\mu \bar{\nu}_\mu \\ \pi^0 &\rightarrow \gamma\gamma. \end{aligned} \quad (35)$$

5.1. Supernova remnants

Cosmic Rays are believed to be produced in young supernova remnants (SNRs), reaching maximum energies of around 10^{15} eV or above, depending on their local environment and on the cosmic ray composition. The production of secondaries from hadronic interactions depends on the proton-proton optical depth in the SNR environment. In this section, we present a model of which sources are optically thin and which, in contrast, are good candidates for the production of high-energy photons and neutrinos.

5.1.1. Optical depth

We use the observation of synchrotron radiation from shock-accelerated electrons, assuming that electrons and hadrons are accelerated in the same shock environment. Figure 7 shows the distribution of spectral indices at radio wavelengths between 1.4 GHz and 5 GHz for 105 sources in the sample with given spectral indices at the required wavelengths. The spectrum at these energies is produced by electron synchrotron losses. Depending on the shape of the primary electron spectrum and scattering effects, the spectral index of the electron population

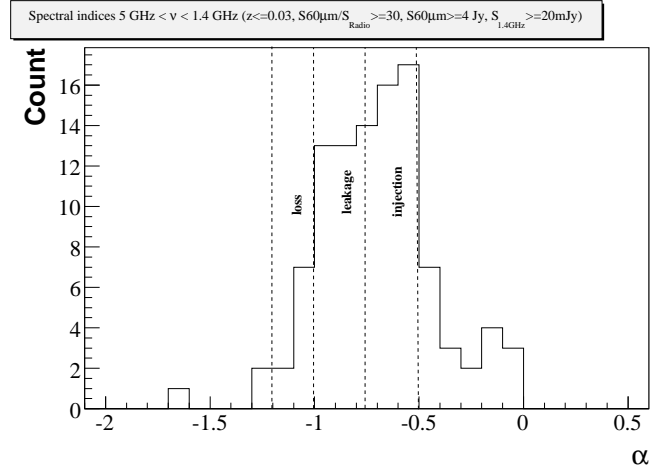


Fig. 7. Histogram of the radio spectral indices of 105 sources between 1.4 GHz and 5 GHz. The areas between the dashed lines indicate sources in the loss, leakage and injection limit (from the left). As a conservative estimate, we include those three sources with extremely steep spectra as loss limit sources. Those sources with extremely flat spectra, to the right of the injection limit area, are dominated by absorption or free-free radiation.

can reach different values. Shock acceleration of charged particles usually results in primary electron spectra of

$$\frac{dN_e}{dE_e} \propto E_e^{-\alpha_e^{\text{prim}}}, \quad (36)$$

with $\alpha_e^{\text{prim}} \approx 2.0 - 2.4$. If the electrons escape before interacting with the ambient medium, the primary spectrum stays unmodified, $\alpha_e^{\text{prim}} = \alpha_e^{\text{sec}}$, referred to as the *injection limit*. If the electrons are partly scattered down to lower energies, the spectrum of secondaries steepens to $\alpha_e^{\text{sec}} \approx 2.5 - 2.8$ for a primary spectrum with $\alpha_e^{\text{prim}} \approx 2.0 - 2.4$. This is called the *leakage limit*. In the case of calorimetric sources, basically the entire energy is lost in the source and the spectrum of secondary electrons is as steep as $\alpha_e^{\text{sec}} \approx 3.2 - 3.4$. This scenario is referred to as the *loss limit*.

As discussed in Rybicki & Lightman (1979), the electron spectral index α_e^{sec} correlates with the index of synchrotron radiation as

$$\alpha = -\frac{\alpha_e^{\text{sec}} - 1}{2}. \quad (37)$$

Thus, the observed synchrotron spectral indices are

$$\alpha = \begin{cases} -0.5 \rightarrow -0.75 & \text{in the } \textit{injection limit} \\ -0.75 \rightarrow -1.0 & \text{in the } \textit{leakage limit} \\ -1.0 \rightarrow -1.2 & \text{in the } \textit{loss limit}. \end{cases} \quad (38)$$

The synchrotron spectral indices in this sample scatter between $-1.7 < \alpha < 0.7$ with a peak at $\alpha \sim -0.7$. We exclude sources that may include contributions other than synchrotron radiation, i.e. those sources that have spectral indices $\alpha > -0.5$. Here, absorption is likely to have modified the spectrum. Alternatively, spectral indices around -0.1 point to free-free radiation (Mezger & Henderson, 1967). Of the remaining 85 sources, 37 sources (44%) starbursts are in the injection limit, 36 sources (42%) are in the leakage limit and 12 sources (14%) are in the loss limit.

The observation of a synchrotron spectrum following the injected electron spectrum has severe implications for hadrons in

the same source. As proton interactions require much higher particle or electromagnetic field densities than electron interactions, it can be expected that hadrons are not affected if electrons can escape freely. Thus, protons escape from the source before they interact. Even in the leakage limit, it is unlikely to have proton interactions with matter or photons, only sources in the loss limit provide conditions with reasonable densities for proton interactions. In the case of high particle densities, protons interact with each other and produce pions as described in Equations (33) and (35). Hence, only those 14% of all starburst sources in the loss limit are likely to produce both high-energy neutrinos and photons. We will take this into account in all following calculations by applying a factor of $\epsilon_{loss} = 0.14$, so that only loss limit sources are included.

5.1.2. Contributions of starbursts to the FIR background

In a previous estimate of high-energy neutrino radiation from starburst galaxies by (Loeb & Waxman, 2006), it is assumed that the entire background of far infra-red radiation comes from starburst galaxies. However, it is pointed out by Stecker (2007) that only a fraction of 23% the total diffuse FIR background actually originates from starbursts. This would reduce the flux of hadronic secondaries by a factor $\xi_{FIR} = 0.23$. Still, as it is pointed out by Thompson et al. (2006), a fraction near unity, $\xi_{FIR} \approx 1$, is consistent with most star formation rate models today and should be considered as an upper limit estimate. In this paper, we will use the FIR background from the EBL model given by (Kneiske et al., 2002), where a total of 80% comes from starbursts.

5.1.3. Production of hadronic secondaries

The non-thermal radio emission from starburst galaxies indicates the shock acceleration of electrons. Hadrons are accelerated in the same way. In the case of proton interactions, high-energy neutrinos and photons can be produced as indicated in Equations (33) and (35). For heavier nuclei, the efficiency is slightly less than for protons due to photo-disintegration, see e.g. Hooper et al. (2005); Ave et al. (2005); Anchordoqui et al. (2008). In this paper, we calculate secondary spectra from protons, and consider heavier cosmic rays elsewhere. High-energy photon emission can also be due to bremsstrahlung or inverse Compton scattering, but above 1 GeV, pion decay photons should dominate as discussed in Paglione et al. (1996); Domingo-Santamaría & Torres (2005). Here, we re-calculate the possible neutrino and photon fluxes for those sources optically thick to proton-proton interactions. Normalization, spectral behavior and propagation are treated as follows:

– Spectral behavior

We assume that the protons at the source follow a power-law spectrum with an index α_p and with exponential cutoff at E_{max} ,

$$\frac{dN_p}{dE_p} = A_p \cdot E_p^{-\alpha_p} \cdot \exp\left[-\frac{E_p}{E_{max}}\right]. \quad (39)$$

The normalization of the spectrum A_p is determined by assuming that a fraction of the total SNR energy, η , goes into cosmic rays. This is described in more detail in the next paragraph. The observed spectrum of cosmic rays below the knee, i.e. below 10^{15} eV is typically assumed to come from supernova explosions in the Galaxy, with a cutoff at 10^{15} eV. The spectral part between the knee and the

ankle of the cosmic ray spectrum is still a matter of debate, but may arise from the heavy particle component from SNRs, see (Stanev et al., 1993). Here, we assume that SNRs in starburst galaxies produce similar spectra. Protons are likely to have an energy cutoff even below 10^{15} eV. As the exact cutoff energy is not known, we use $E_{max} = 10^{15}$ eV as an upper limit. The observed spectral index is $\alpha_p = 2.7$. Stochastic particle acceleration usually produces spectra of around $2.0 < \alpha_p < 2.4$. Hence, it is not sure yet where the steepening of the spectrum occurs, whether it is an internal steepening or a propagation effect. We therefore test proton spectra with indices of $\alpha_p = 2.7, 2.4, 2.2, 2.0$. A spectrum of $E^{-2.7}$ would be present when diffusion applies, spectral indices between 2.0 and 2.4 are predicted by stochastic acceleration without significant diffusion. This approach differs from the calculations by Paglione et al. (1996); Domingo-Santamaría & Torres (2005), who use the diffusion-loss equation to determine the spectral index.

In all following calculations, we determine the spectra of hadronic secondaries from proton-proton interactions, using the delta-functional approximation for proton energies $E_p < 100$ GeV, see e.g. (Mannheim & Schlickeiser, 1994). At higher energies, the more exact analytic approximation as presented in Kelner et al. (2006) is used, where Monte-Carlo simulation results are approximated by analytical equations. For all energies, the logarithmic increase of the proton-proton cross section with energy is taken into account as described in Kelner et al. (2006). We have a high hydrogen density, $n_H = 100 \text{ cm}^{-3}$, as we expect the dominant proton acceleration and interaction to occur in heavy supernova remnants, having red supergiants or Wolf-Rayet stars as progenitors.

– Normalization

We normalize the energy spectrum of cosmic rays by determining their energy density ρ_{CR} . The latter is defined by the energy integration over the differential cosmic ray flux, multiplied with the energy, multiplied by a factor $4\pi/c$ to get from a flux to a density,

$$\rho_{CR} := \frac{4\pi}{c} \int_{E_{min}}^{\infty} dE_p \frac{dN_p}{dE_p} \cdot E_p. \quad (40)$$

In order to determine the normalization of the total proton flux from starbursts, we assume a power-law spectrum with an exponential cutoff as described in Equ. (39).

The energy density, in turn, is directly proportional to the supernova rate in a galaxy, \dot{n}_{SN} , assuming that a fraction η of the total energy of a supernova, $E_{SNR} \approx 10^{51}$ erg is transferred to cosmic rays,

$$\rho_{CR} = \frac{\epsilon_{loss} \cdot \eta \cdot E_{SNR} \cdot \dot{n}_{SN}}{c \cdot d_l^2(z) \cdot (1+z)^2}. \quad (41)$$

Here, we use $\epsilon_{loss} = 0.14$ as discussed in Sections 5.1.1 and 5.1.2. We further assume that 5% of the total SNR energy is transferred to cosmic rays, i.e. $\eta = 0.05$. To determine the supernova rate in a galaxy, the total FIR luminosity at a given redshift z , $L_{FIR}^{tot}(z)$, is estimated from the FIR emissivity $\mathcal{E}_{FIR}(z)$, the latter coming from the extragalactic background light (EBL) model from Kneiske et al. (2002),

$$L_{FIR}^{tot} = \int \mathcal{E}_v^{FIR}(z) \frac{dV}{dz}(z) dv. \quad (42)$$

Here, dV/dz is the comoving volume element.

quantity	variable	value
total energy release (SNR)	E_{SNR}	10^{51} erg
energy fraction transferred from SNR to CRs	η	0.05
hydrogen density	n_H	100 cm^{-3}
fraction of starbursts in the loss limit	ϵ_{loss}	0.14

Table 2. Parameters used to determine the diffuse flux of high-energy photons and neutrinos from SNRs in starburst galaxies.

The supernova rate was determined by Mannucci et al. (2003) to correlate with the FIR luminosity of the galaxy,

$$\dot{n}_{SN} = (2.4 \pm 0.1) \cdot 10^{-12} \cdot \left(\frac{L_{FIR}}{L_{\odot}} \right) \text{ yr}^{-1}. \quad (43)$$

The FIR luminosity is expressed in terms of the solar luminosity, $L_{\odot} = 3.839 \cdot 10^{33}$ erg/s. This relation was predicted in (Biermann & Fricke, 1977; Kronberg & Biermann, 1981) within a factor of 3, and other experimental results from van Buren & Greenhouse (1994) yield the same correlation within uncertainties. Finally, the cosmic ray energy density is given as

$$\rho_{CR} = 1.6 \cdot 10^{-13} \text{ erg/cm}^3 \cdot \epsilon_{loss} \cdot \frac{\eta}{0.05} \cdot \frac{E_{SNR}}{10^{51} \text{ erg}} \cdot \frac{L_{FIR}}{10^{12} L_{\odot}} \cdot \left(\frac{d(z)}{6.5 \text{ Gpc}} \right)^{-2} \cdot \left(\frac{1+z}{2} \right)^{-2}. \quad (44)$$

This number is compatible with the observed cosmic ray spectrum above 1 GeV in the Galaxy, $\rho_{CR}^{MW} = 1 \text{ eV/cm}^3$, assuming a supernova rate of $\dot{n}_{SN} = 0.03/\text{yr}$.

– Propagation

We apply that the particle energy at Earth is a factor of $1+z$ higher than at the source. Neutrinos travel in straight lines without interaction. In the case of photon propagation, we include absorption effects by the EBL, using the model of Kneiske et al. (2002).

From the considerations above, the spectra of hadronic secondaries at Earth from a given redshift z are determined and a simple redshift integration is performed in order to get the total neutrino flux at Earth. Here, we integrate from $z = 0$ up to a redshift where first starbursts are expected to be formed. We use $z_{\max} = 5$, since the main contribution to the spectra comes from redshifts up to $z \sim 1 - 2$. The contribution above $z = 5$ is negligible.

5.1.4. High-energy photons

Assuming proton-proton interactions in starbursts as described above, we calculate the gamma-ray emission produced by starburst galaxies for energies > 1 GeV. A detailed calculation and discussion for the starburst galaxy NGC253 has been done in Paglione et al. (1996); Domingo-Santamaría & Torres (2005). Gamma-ray emission in starburst galaxies is due to three different processes, Bremsstrahlung, inverse Compton scattering and pion decay. In the following only gamma-ray emission from pion decay is considered because it is the dominating process at energies above 1 GeV (Paglione et al., 1996; Domingo-Santamaría & Torres, 2005).

In Fig. 8, the model of gamma-ray emission from starbursts as presented above is shown for three different proton spectra,

i.e. $E^{-2.0}$ as the thick solid, $E^{-2.2}$ as the thick dashed, $E^{-2.4}$ as the thick dot-dashed and $E^{-2.7}$ the thick dotted line. We use that only 14% of all starbursts are in the loss limit ($\epsilon_{loss} = 0.14$) and we apply the FIR background from the EBL model by Kneiske et al. (2002). Absorption due to the EBL is considered in all calculations. We compare our results to the observation of the diffuse, extragalactic background as measured by EGRET (Sreekumar et al., 1998). Closed squares represent the first analysis presented in Sreekumar et al. (1998), while open circles show an updated analysis, using an improved model for the distraction of the galactic component from the extragalactic contribution (Strong et al., 2005). The high-energy radiation from starburst galaxies makes up about 10% percent of the total background. In the same figure, we show other possible contributions to the total diffuse background, like the one from resolved EGRET blazars (Kneiske & Mannheim, 2008) or the contribution from regular galaxies (Pavlidou & Fields, 2002). Karlsson (2008) present a model of high-energy photon emission from starbursts. Just as Karlsson (2008), we include the logarithmic rise of the proton-proton cross section with energy and get comparable results. In addition, our results yield a slightly lower flux than the prediction by Thompson et al. (2007). The main reason is that we include that only 14% of all starbursts are proton calorimeters where Thompson et al. (2007) assume that this fraction increases from 10% for local starbursts to a saturated value of 80% at $z = 1$. We use this more conservative approach. The considerations above show that several factors are quite uncertain, i.e. the total energy released by a supernova remnant, the hydrogen density, as well as the number of starburst galaxies that contribute to the FIR background and that are proton calorimeters. Thus, the possibility of starbursts contributing significantly to the diffuse photon background at high energies should be considered. The Fermi satellite², launched on June 11, 2008, will help identifying starburst galaxies at energies above 100 MeV, to determine the exact fraction of the starburst diffuse photon flux in the total gamma background.

5.1.5. High-energy neutrinos

The high-energy neutrino flux calculated according to Section 5.1.3 is presented in Fig. 9, for an $E^{-2.0}$, $E^{-2.2}$, $E^{-2.4}$, $E^{-2.7}$ (thick solid, dashed, dot-dashed and dotted lines) spectral behavior of the initial proton spectrum. Although, in contrast to Loeb & Waxman (2006), we take into account that only 14% of all sources are effective proton calorimeters, the flux strength of our prediction is compatible with Loeb & Waxman (2006): While Loeb & Waxman (2006) use the radio luminosity of local starbursts as an estimate, we take the supernova rate as a measure. The reason for the cutoff at lower energies is that we assume that protons are not accelerated beyond 10^{15} eV, which is based on the observation of the knee in cosmic rays at about 10^{15} eV. The interpretation that SNRs in the Galaxy are responsible for the flux below 10^{15} eV justifies the assumption that also in starbursts, SNR accelerate cosmic rays up to similar energies. It should be kept in mind, however, that the actual cutoff for protons is likely to lie at energies below 10^{15} eV and that only heavier cosmic rays, which we do not consider in this calculation, can reach energies as high as 10^{15} eV. With an energy cutoff at or below 10^{15} eV, the neutrino flux from starbursts is out of reach for the detection of a diffuse flux by high-energy neutrino detectors like Km3NeT and IceCube as indicated in Fig. 9.

² called GLAST before its launch

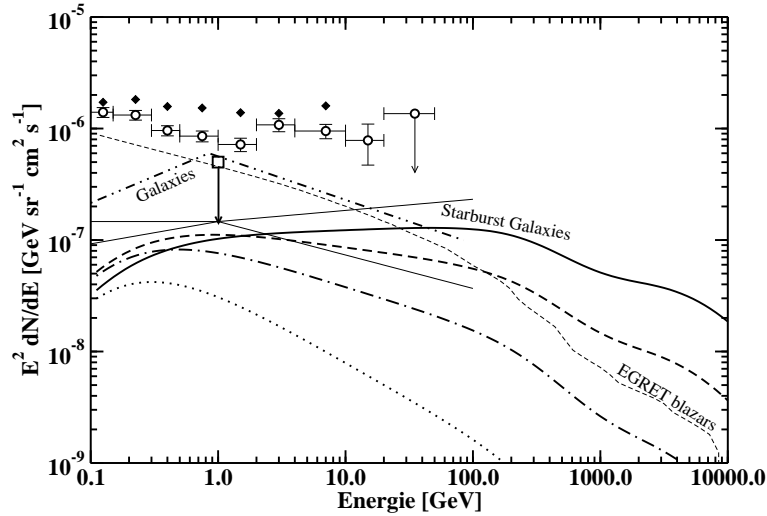


Fig. 8. Expected diffuse high-energy photon flux from SNRs in starburst galaxies. The black lines represent the contribution for an E^{-2} (thick, solid), $E^{-2.2}$ (thick, dashed), $E^{-2.4}$ (thick, dot-dashed) and $E^{-2.7}$ (thick, dotted) proton input spectrum with an exponential cutoff at 10^{15} eV. Closed data points are from the EGRET experiment (Sreekumar et al., 1998). Open data points represent an update of the EGRET data, using an updated model for galactic gamma-ray emission (Strong et al., 2005). The thin, dashed line represents the contribution from EGRET blazars (Kneiske & Mannheim, 2008). The thin, dot-dot dashed line shows the possible contribution from regular galaxies (Pavlidou & Fields, 2002), while the thin, solid lines display contribution from starbursts as calculated by Thompson et al. (2007), E^{-2} and $E^{-2.3}$ initial proton spectra.

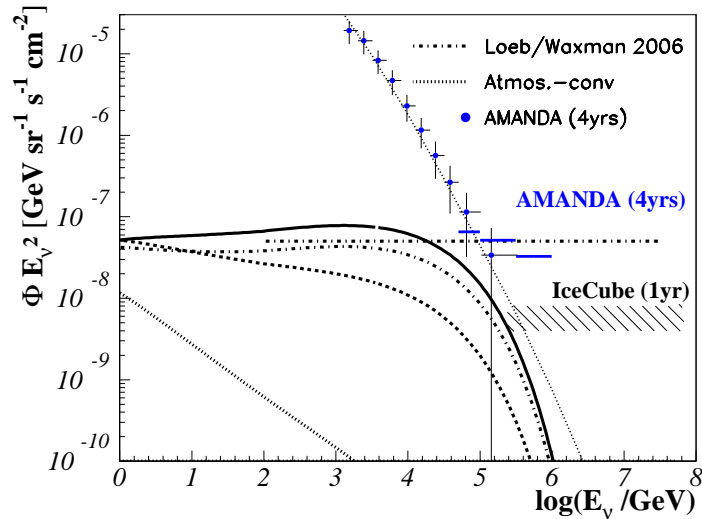


Fig. 9. Expected diffuse high-energy neutrino flux from SNRs in starburst galaxies. The black lines represent the contribution for an E^{-2} (thick, solid), $E^{-2.2}$ (thick, dashed), $E^{-2.4}$ (thick, dot-dashed) and $E^{-2.7}$ (thick, dotted) proton input spectrum with an exponential cutoff at 10^{15} eV. Data points show the atmospheric neutrino background as measured by the AMANDA experiment (data between 2000 and 2003) Münich et al. (2007); Münich (2007). The prediction of atmospheric neutrinos is taken from Volkova (1980). AMANDA limits are for the same data sample, derived from the fact that no significant excess above the atmospheric background was observed. The dot-dashed line shows the prediction by Loeb & Waxman (2006), not taking into account that only 14% of all starbursts are calorimeters.

5.2. Gamma Ray Bursts

As starburst galaxies show an enhanced rate of supernova explosions, an increased rate of long Gamma Ray Bursts (GRBs), which are directly linked to SN-Ic events (Mazzali et al., 2003, e.g.), is expected. Thus, if long GRBs are the dominant sources of UHECRs, the contribution from nearby objects should fol-

low the distribution of starburst galaxies. Here, we examine the number of GRBs to be expected from our catalog.

In the following calculations, we assume that every SN-Ic explosion is accompanied by a particle jet along the former star's rotation axis, i.e. by a GRB. The opening angle of the GRB jet θ determines, how many SN-Ic can be observed as GRBs,

$$\dot{n}_{\text{GRB}} = \epsilon \cdot \dot{n}_{\text{SN-Ic}}. \quad (45)$$

Here, \dot{n}_{GRB} is the GRB rate in a galaxy and $\epsilon = (1 - \cos \theta)$ is the fraction of SN-Ic producing GRBs. The jet opening angle is difficult to determine. Typically, one expects an opening angle of less than 10° for the prompt emission, see e. g. Berger et al. (2003); Racusin et al. (2008). Afterglow emission and precursors can have larger opening angles (Morsony et al., 2007). As we focus on the prompt emission, we will use a typical opening angle of $\sim 10^\circ$ as an optimistic estimate, i.e.

$$\epsilon \approx 0.015. \quad (46)$$

Further, observational data show that core collapse supernovae of type SN-Ib/c contribute with 11% to the total SN rate in starbursts (Cappellaro & Turatto, 2001). Thus, using Equ. (45), the GRB rate in a starburst galaxy is directly correlated to the supernova rate \dot{n}_{SN} ,

$$\dot{n}_{\text{GRB}} = \epsilon \cdot \zeta \cdot \dot{n}_{\text{SN}}, \quad (47)$$

with $\zeta \sim 0.11$ as the fraction of heavy SN explosions in all SN explosions in a single galaxy. Using Equ. (43) to determine the supernova rate in a galaxy in Equ. (47) yields a GRB rate of

$$\dot{n}_{\text{GRB}} = 3.8 \cdot 10^{-15} \cdot \left(\frac{L_{\text{FIR}}}{L_\odot}\right) \cdot \left(\frac{\epsilon}{0.015}\right) \cdot \left(\frac{\zeta}{0.11}\right) \text{yr}^{-1} \quad (48)$$

per starburst. With an expected lifetime of more than 10 years for a neutrino detector like IceCube, luminosities of around $3 \cdot 10^{13} \cdot L_\odot \sim 10^{47}$ erg/s are required for the detection of a single event. None of the sources in our catalog provides such high luminosities: IRAS17208-0014 is the intrinsically strongest source with $L_{\text{FIR}} = 5.9 \cdot 10^{45}$ erg/s, the second strongest one is IRASF17207-0014 with $L_{\text{FIR}} = 5.5 \cdot 10^{45}$ erg/s. If, however, a larger number of starbursts is considered for an analysis, the total luminosity increases and with it the probability of observing a GRB. Figure 10 shows the total GRB rate for a number of $N_{\text{starbursts}}$ galaxies,

$$\dot{n}_{\text{GRB}}^{\text{tot}}(N_{\text{starbursts}}) = \sum_{i=1}^{N_{\text{starbursts}}} \dot{n}_{\text{GRB}}(i\text{th starburst}). \quad (49)$$

In the figure, we sum up the GRB rates achieved in the single starbursts, starting with the most luminous source, adding sources in descending luminosity order. The red points show the GRB rate summing over all starbursts in the sample. On total, 0.03 GRBs per year are expected to be observable from our sample of starbursts. The blue squares display the total GRB rate, summing up sources in the northern hemisphere, which corresponds to IceCube's Field of View (FoV), in order to estimate the neutrino detection probability in Section 5.2.2. Here, 0.02 GRBs per year are expected. This number can be enhanced significantly when taking into account those weaker sources which we do not include in our catalog in order to ensure completeness (see Section 3).

5.2.1. Observation of cosmic rays and starburst galaxies

Of the 127 sources in our catalog, 96 are located in the northern hemisphere. Thus, Auger South will only have very few starbursts in its FoV, while HiRes, the Telescope Array (TA) and later Auger North will be able to observe a large fraction of starbursts. As already discussed by Biermann et al. (2008), the question of the origin of UHECRs can only be resolved by taking this strongly asymmetric distribution into account. Even if GRBs contribute to the total flux of cosmic rays, nearby sources cannot be identified by a southern hemisphere telescope, since

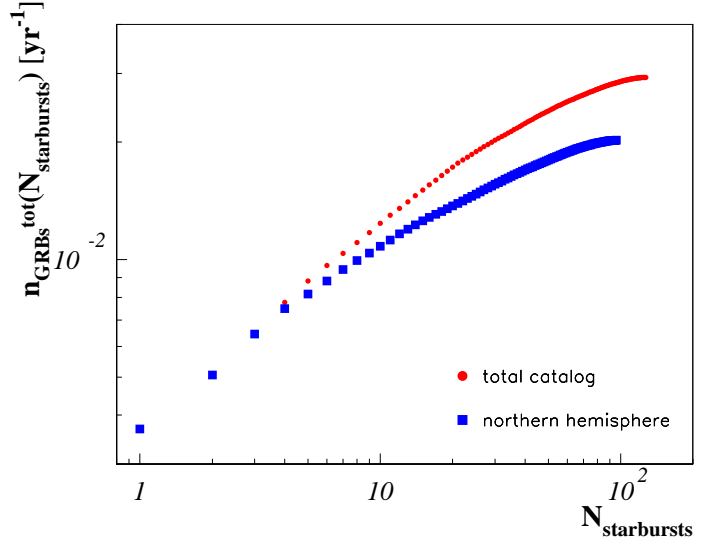


Fig. 10. Number of GRBs per year in the starburst catalog, including $N_{\text{starbursts}}$ sources, starting with the strongest one. Red circles include all starbursts in the sample. The total GRB rate in the sample, including all 127 sources, is 0.03 yr^{-1} , which means that a GRB could be observed every 30 years on average. Results shown in blue squares only show northern hemisphere bursts, lying in the IceCube FoV. Northern hemisphere GRBs would occur every 50 years ($\dot{n}_{\text{GRB}} = 0.02 \text{ yr}^{-1}$).

the number of sources is too small. Given the large number of sources in the northern hemisphere, telescopes like HiRes, TA and Auger North can investigate this matter. In particular, for GRBs coming from one of the starbursts in our catalog could give the opportunity of an enhanced UHECR flux within a short time window, assuming that the signal is still focused in time and space due to the closeness of the sources. Thus, an analysis with UHECR detectors in the northern hemisphere for nearby GRBs could be optimized by not only looking for spatial but also for temporal clustering.

5.2.2. Enhanced neutrino flux from GRBs in starbursts

While the detection of a permanent, diffuse signal from GRBs in nearby starbursts will not be possible due to the high atmospheric background seen by high-energy neutrino telescopes, a timing analysis may be able to identify the Gamma Ray Bursts in neutrinos. In such an analysis, the location of a nearby starburst can be chosen as a potential neutrino hot-spot. By defining a time window of the typical duration of a long GRB (~ 100 s), the atmospheric background can be reduced to close to zero. The GRB event rate per starburst galaxy was already examined above. Here, the general neutrino intensity and in particular the possibility of detection with IceCube are discussed.

Neutrino spectrum from a single GRB in a starburst The neutrino spectrum during the prompt photon emission phase in a GRB was for the first time determined by Waxman & Bahcall

(1997, 1999). It can be expressed as a broken power-law,

$$\frac{dN_\nu}{dE_\nu} = A_\nu \cdot E_\nu^{-2} \cdot \begin{cases} E_\nu^{-\alpha_\nu+2} \cdot \epsilon_\nu^{b\alpha_\nu-\beta_\nu} & \text{for } E_\nu < \epsilon_\nu^b \\ E_\nu^{-\beta_\nu+2} & \text{for } \epsilon_\nu^b < E_\nu \leq \epsilon_\nu^s \\ \epsilon_\nu^s \cdot E_\nu^{-\beta_\nu+1} & \text{for } E_\nu > \epsilon_\nu^s. \end{cases} \quad (50)$$

The spectrum includes the five parameters α_ν , β_ν , ϵ_ν^b , ϵ_ν^s , A_ν . We discuss the numerical values of the parameters below. For their derivation, see e.g. Guetta et al. (2004); Becker et al. (2006). The derivation is done for an isotropically emitted signal. However, the neutrino spectrum itself does not vary with the jet's opening angle, since the parameters are determined by energy densities. Where the energy is enhanced by a factor $1/(1 - \cos\theta)$, the solid angle decreases just as $(1 - \cos\theta)$ and the factors cancel.

– *The break energies ϵ_ν^b and ϵ_ν^s*

The neutrino spectrum can be derived when assuming that the protons accelerated along the GRB jet interact with the ambient synchrotron photon field. Neutrinos are produced in π^+ -decays as described in Equ. (35). The first break energy represents the energy required to produce the Delta resonance in proton-photon scattering. At higher energies, $E_\nu > \epsilon_\nu^b$, the neutrino spectrum follows the proton spectral behavior, $\beta_\nu \sim \alpha_p$. At lower energies, $E_\nu < \epsilon_\nu^b$, scattering becomes less effective and the spectrum becomes flatter, $\alpha_\nu \sim \alpha_p - 1$. Due to the transformation from the CM system of the proton-photon interaction in the source into the observer's frame at Earth, the first break energy depends on the shock's boost factor $\Gamma := 10^{2.5} \cdot \Gamma_{2.5}$, the observed photon break energy of GRBs and the redshift ($z \approx 0$ for our catalog),

$$\epsilon_\nu^b = 7 \cdot 10^5 \cdot (1+z)^{-2} \frac{\Gamma_{2.5}^2}{\epsilon_{\nu, MeV}^b} \text{ GeV} \approx 3 \cdot 10^6 \text{ GeV}. \quad (51)$$

We fix the boost factor to $\Gamma_{2.5} = 1$ and the observed photon break energy to $\epsilon_{\nu, MeV}^b := \epsilon_\nu^b / \text{MeV} \sim 0.25$. For the sources in our catalog, we have $z \approx 0$.

The second break in the neutrino spectrum, due to pion-synchrotron losses, is determined by unknown parameters like variability time scale $t_\nu \approx 0.01 \text{ s} \cdot t_{\nu,-2}$, GRB luminosity $L_\gamma \sim 10^{51} \text{ erg/s} \cdot L_\gamma^{51}$ and electron and magnetic field equipartition fractions, $\epsilon_e \approx \epsilon_B \approx 0.1$.

$$\epsilon_\nu^s = \frac{3 \cdot 10^7}{1+z} \epsilon_e^{1/2} \epsilon_B^{-1/2} \Gamma_{2.5}^4 t_{\nu,-2} / \sqrt{L_\gamma^{51}} \text{ GeV} \approx 3 \cdot 10^7 \text{ GeV}. \quad (52)$$

Here, we fix the parameters to $t_{\nu,-2} = 1$, $L_\gamma^{51} = 1$, $\epsilon_B = \epsilon_e = 0.1$.

– *The spectral indices α_ν and β_ν .*

In the energy range $\epsilon_\nu^b < E_\nu < \epsilon_\nu^s$, the spectral index $\beta_\nu = p$ is represented by the primary hadron spectral index. We assume a simple E^{-2} proton spectrum in this case: While it was argued previously, that highly relativistic flows have a limit of not becoming flatter than $\sim E^{-2.2}$ (Bednarz & Ostrowski, 1998), recent studies of oblique shocks have shown that particle spectra as flat as $E^{-1.5}$ can be produced with shock boost factors of $\Gamma > 100$ as they occur in GRBs, see Meli et al. (2008). In addition, including large angle scattering of particles in the acceleration process also leads to flat particle spectra, see Stecker et al. (2007). This implies, the exact spectral index depends on the shock properties. As we are not dealing with observed GRBs here, but with potentially

to-be-observed GRBs, we cannot determine the spectral behavior by the observation of the synchrotron spectrum as it was done in Guetta et al. (2004); Becker et al. (2006). Thus, we use $\alpha_\nu = 1$ and $\beta_\nu = 2$ as a first order approximation, just as it is done in several approaches of unknown single-source spectra, see e.g. (Waxman & Bahcall, 1997, 1999).

– *The normalization A_ν*

The normalization, which corresponds to the intensity of the burst, is given by

$$A_\nu = \frac{1}{8} \frac{1}{f_e} \frac{E_\gamma^{iso}}{4\pi \cdot d_L^2} \cdot \frac{f_\pi}{\ln(10)}. \quad (53)$$

Here, we use a fixed isotropic energy release of $E_\gamma^{iso} = L_\gamma \cdot t_{90} = 10^{52} \text{ erg}$, where we assume a burst duration of $t_{90} \approx 10 \text{ s}$. Further, we assume that the energy contained in GRB electrons is 1/10th of the energy contained in GRB protons, $f_e = 0.1$. The factor $f_\pi \approx 0.2$ describes the fraction of energy transferred to the charged pion. The factor 1/8 is applied since 1/2 of all proton-photon interactions go into neutrino production, and 1/4 goes into a single neutrino flavor. Here, we fix all parameters except for the distance d_L of the GRB from Earth, which is determined by the distance of the starburst from Earth.

To estimate the neutrino flux from a standard GRB from one of the starburst galaxies in our sample, we simply calculate a normalization, dependent on the distance of the starburst. Every other parameter is kept constant. Hence, the results can only serve as a rough estimate of what would happen on average. Both the spectral indices, the break energies and the normalization fluctuate with each burst as described theoretically in Guetta et al. (2004); Becker et al. (2006) and worked out experimentally in AMANDA for the case of GRB030329 (Stamatikos et al., 2005) and in IceCube for GRB080319B (Kappes et al., 2008). One of the most important parameters is the total GRB energy. Here, we assume that it is $E_\gamma^{iso} = 10^{52} \text{ erg}$. The isotropic equivalent energy for the 'naked eye' GRB080319B is two orders of magnitude higher, i.e. $1.3 \cdot 10^{54} \text{ erg}$ and several weak bursts will have smaller isotropic equivalent energies. While these effects cannot be taken into account due to lack of knowledge, they should be kept in mind. In case of a positive detection in a high-energy neutrino detector, the parameters can of course be determined explicitly. In the case of a negative result, it would be possible to set a limit in the following sense: no GRB with isotropic equivalent luminosities occurred during the time of observation in the given starburst(s).

Expected events in IceCube The probability of a GRB to be observed from one of the starburst galaxies in the sample from the northern hemisphere is shown in Fig. 10 (blue squares). Analyzing all 96 sources in the northern hemisphere, a rate of

$$\dot{n}_{\text{GRB}}^{\text{total/north}} (N_{\text{starbursts}} = 96) = 0.02 \text{ yr}^{-1} \quad (54)$$

is expected. This number can be enhanced significantly when we consider all starbursts originally selected (309 sources). We only consider the brightest ones for completeness reasons. Thus, we expect that at least one GRB from a starburst in the supergalactic plane should happen in the lifetime of IceCube, if not more. Prospects for Km3NeT are not as optimal as for IceCube, since Km3NeT will be located in the northern hemisphere, looking at the southern sky, and the instrument will therefore only see

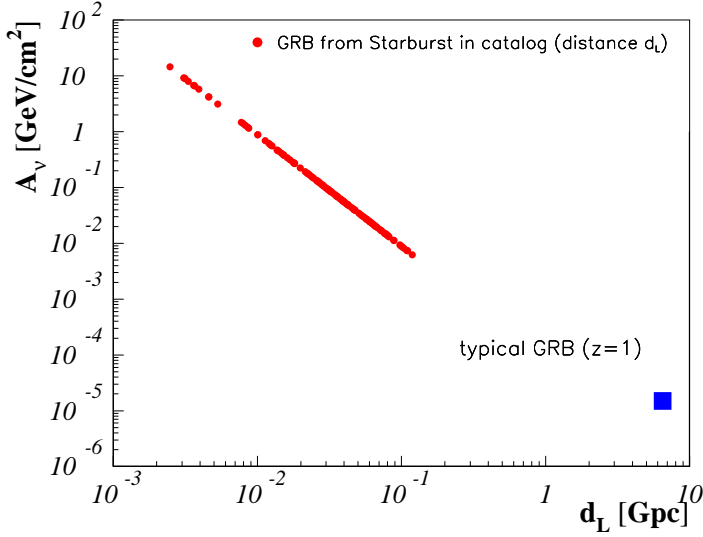


Fig. 11. Neutrino intensity A_ν for a single GRB from a starburst at a luminosity distance d_L . A generic GRB isotropic energy of $E_\gamma^{iso} = 10^{52}$ erg is assumed. Therefore, the neutrino intensity only depends on the luminosity distance as $A_\nu \propto d_L^{-2}$.

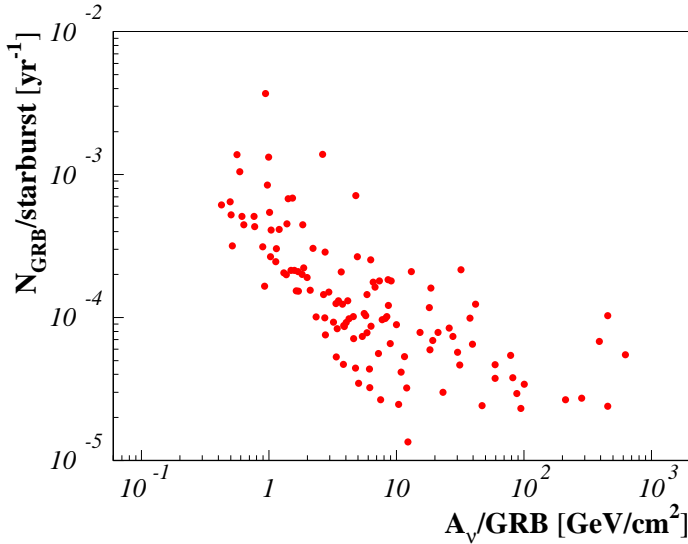


Fig. 12. Number of GRBs in a starburst versus neutrino flux intensity for each starburst. The sharp cutoff at low neutrino intensities comes from the distance cut performed at $z = 0.03$. This leads to a cutoff in the neutrino intensity, since the latter is proportional to the luminosity distance squared.

a small fraction of the class of starburst galaxies, which dominantly shows sources in the northern hemisphere.

IceCube's effective area A_{eff} is presented by Montaruli et al. (2007) and can be used to determine the total number of events per GRB in IceCube, N_{events} , by folding it with the GRB spectrum dN_ν/dE_ν ,

$$N_{events} = \int_{E_{th}}^{\infty} A_{eff}(E_\nu) \cdot \frac{dN_\nu}{dE_\nu}(E_\nu) dE_\nu. \quad (55)$$

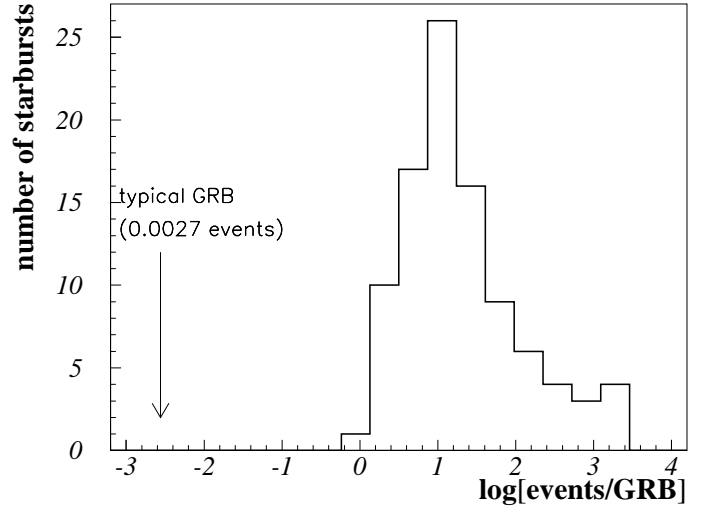


Fig. 13. Histogram of number of events in IceCube from the 96 starburst galaxies in the northern hemisphere. The IceCube effective area we use (Montaruli et al., 2007) does not take into account sensitivity changes with declination. All bursts are stronger than 1 event in IceCube, since they come from starbursts closer than $z = 0.03$. For more distant bursts, the number of events will be less, since the neutrino intensity decreases with the distance squared.

Here, we neglect the weak dependence of the effective area on the declination of the burst. For the threshold energy, we use $E_{th} = 100$ GeV (Ahrens et al., 2004). This is the general detection threshold of IceCube. As events can be selected by direction and a small time window, the atmospheric background can be reduced to almost zero. Therefore, events in the entire energy range are available in such an analysis. If we now assume a standard burst with an isotropic energy release of $E_\gamma^{iso} = 10^{52}$ erg, we can estimate how strong a GRB would be on average from the nearby starbursts in our catalog. Figure 13 shows the histogram of the number of events per starburst for an average GRB. Depending on the distance of the starburst, the event rate in IceCube ranges from more than 1 event up to more than 1000 events per burst in a small time window of around 10 – 100 seconds. These numbers lie between 2 and 6 orders of magnitude above those GRBs typically observed by satellite experiments like BATSE, Swift and Fermi. The reason why such a strong burst has not been observed in gamma-rays is simply the relatively low rate of occurrence³. If such an event happens, neutrino detectors, and also cosmic ray detectors have a higher chance of detection due to their extremely large FoV ($\sim 2\pi$).

5.2.3. High-energy photons and nearby GRBs

Following the channel of π^0 production rather than the neutrino-producing charged pions, we see that a high-energy photon signal is always expected along with high-energy neutrino emission. Such a correlation could be observed for sources optically

³ The exact number cannot be given here, since we only consider those sources with relatively high fluxes in the radio and at FIR wavelengths. The total rate of 0.02 GRBs/year could be enhanced significantly with a lower flux threshold.

thin to TeV photons. In such a case, GRBs in nearby starburst galaxies would produce an equally strong signal in neutrinos as in high-energy photons. This means a good discovery potential for large FoV detectors at GeV-TeV energies. Fermi is one of the best candidates to observe this high-energy radiation at GeV energies, Milagro and its successor HAWC will be able to see such events at TeV energies. Air Cherenkov Telescopes like H.E.S.S., MAGIC and VERITAS have a FoV that is too small and are therefore not well-suited for a detection of those rare GRBs. If, however, such a GRB is detected by Swift, especially MAGIC will be able to follow up the GRB quickly, as the telescope is designed for quick GRB follow-ups, see e.g. Galante et al. (2008).

5.2.4. Summary

To sum up, if a GRB will happen in one of the 127 starburst galaxies, the detection probability is extremely high in wide-FoV detectors for high-energy neutrinos and photons as well as in cosmic rays. Since most sources are located in the northern hemisphere, detectors like IceCube, HAWC and Auger are optimal for for such a study. This would enable a detailed study of the hadronic emission processes of GRBs, since the main three messenger particles are covered. Explicit search methods for an enhancement of cosmic rays, high-energy photons and neutrinos from those starbursts can clarify whether or not such a burst happens or not. In the case of the closest sources, the GRB should even be visible in a typical skymap of neutrino, photon or cosmic ray telescopes.

6. Implications and possible experimental tests

In this paper, we present a model to explain the correlation between far-infrared and radio emission in starburst galaxies and we discuss the particle spectra from cosmic ray interactions and possibilities of their observation at Earth. In this context, we also present a catalog of 127 nearby ($z < 0.03$) starburst galaxies with both FIR ($S_{60\mu} > 4$ Jy) and radio ($S_{1.4\text{GHz}} > 20$ mJy) measurements. Those starbursts lie in the supergalactic plane ($z < 0.03$) and serve as a test for basic properties of starbursts. It can further be used to calculate the cosmic ray emission from starbursts in the local Universe. In this section, we summarize implications:

1. FIR-Radio correlation

Within this model, we show that the radio emission is basically independent of the magnetic field strength. This leads to a calorimetric correlation between radio and FIR emission.

Starburst galaxies as well as quiescent galaxies equally obey the correlation between the radio and the far-infrared emission. Therefore the theory implies by necessity that the magnetic field in a starburst region rises with the overall energy density. Since galactic dynamos are not understood, this just raises the ante in terms of the requirements for any theory that tries to account for the magnetic fields and their strengths in galaxies, see (Beck & Hoernes, 1996, e.g.).

Interacting galaxies, subject to substantial compression, show magnetic fields higher than corresponds to the energy density derived from star formation. Therefore, it may be expected that they have more radio emission than indicated by the general radio/FIR correlation. At least one example shows this kind of behavior (Hummel & Beck, 1995).

There is likely also a lowest level of star formation activity, where the assumption that the hot medium is fully connected,

fails. There one may expect also substantial departures from the correlation.

2. *High-energy photons and neutrinos from SNRs in starbursts*
The diffuse high-energy neutrino and photon flux from SNRs in starbursts has been discussed previously by Loeb & Waxman (2006); Thompson et al. (2007). In our calculation, we assume that a fraction of the total energy of a SNR is transferred to cosmic ray acceleration. It is usually assumed that supernova remnants in the Galaxy accelerate particles up to the knee, i.e. $E_{\text{max}} \sim 10^{15}$ eV. Under the assumption that this is the maximum energy for SNRs in starburst galaxies, we show that a detection of the diffuse neutrino flux from starbursts with IceCube or Km3NeT is unlikely. The main reason is the low energy cutoff, and not the strength of the signal. On the other hand, if it were possible to accelerate protons to even higher energies in SNRs in starbursts, as is suggested by Loeb & Waxman (2006), IceCube will be sensitive to the neutrino flux. High-energy photons make up around 10% of the total high-energy photon background observed by EGRET. The high-energy photon detector Fermi was launched on June 11, 2008 and will soon be able to give more details on the background and which sources and source classes contribute. Cosmic rays themselves cannot be observed from starburst galaxies, since the background of Galactic cosmic rays is too high.
3. *High-energy neutrinos and cosmic rays from GRBs in nearby starbursts*

Due to an enhanced rate of star formation and supernova explosions in starbursts, these Galaxies provide a higher probability for Gamma Ray Bursts compared to regular galaxies. So far, Gamma Ray Bursts could not be identified in high-energy neutrinos. Despite their tremendous release of neutrinos, they are usually too far away to yield a significant signal individually ($z \sim 1 - 2$). The stacking of known GRB locations in neutrino data was done with the AMANDA experiment, see Achterberg et al. (2007, 2008), with limits above the typical, expected diffuse flux. IceCube will be able to explore the diffuse neutrino flux using the stacking method. Two single GRBs were also analysed, the first one being GRB030329, using AMANDA data (Stamatikos et al., 2005), the second one being GRB080319B, using IceCube in a 9-string configuration (Kappes et al., 2008). In this paper, we show using our catalog of starbursts in the supergalactic plane, that GRBs in closeby starbursts ($z < 0.03$) typically produce event rates in IceCube above 1 event per bursts. For the most distant sources at $z = 0.03$, about 1 event is expected, for the closest sources, more than 1000 events are predicted within a short time window of a few tens of seconds. In our catalog of 127 starbursts, about 1 GRB is expected each 30th year, most of those happening in the northern hemisphere. The total rate of GRBs in the supergalactic plane is, however, expected to be higher, since we only include the brightest sources in this catalog ($S_{60\mu} > 4$ Jy and $S_{1.4\text{GHz}} > 20$ mJy). The stacking of starburst galaxies for a neutrino analysis would help identifying the sources at $z \sim 0.03$, while the closest sources will immediately be visible in a neutrino skymap. Those GRBs should be accompanied by high-energy photon emission as well. Fermi will be able to identify these at GeV energies (Connaughton, 2007). At even higher energies, Milagro (Vasileiou & (MILAGRO Coll.), 2007) and the next generation experiment HAWC (Sinnis et al., 2005; Smith et al., 2006) will be able to investigate TeV emission. For such nearby and strong cosmic ray emitters, it might even be pos-

sible to identify them in charged cosmic rays, given that diffusion in time and space is not too large.

Acknowledgements. Chapter 4 was distributed as an MPIfR preprint in an earlier version 1995, following a lecture at a conference in Heidelberg. We would like to thank W. I. Axford, R. Beck, A. Bell, E. Berkhuijsen, D. Breitschwerdt, R. Chini, K. Chyży, L. Drury, C. Galea, F. Halzen, M. Harwit, R. Jokipii, A. Kandus, H. Kang, A. Kappes, U. Klein, T. de Jong, P. P. Kronberg, H. S. Lee, J. Mathis, W. M. Matthaeus, H. Meyer, P. G. Mezger, K. Otmianowska-Mazur, V. Ptuskin, M. and G. Rieke, W. Rhode, D. Ryu, T. Schmutzler[†], E.-S. Seo, L. F. Smith, T. Stanev, F. Tabatabaei, M. Tjus, U. Torkelsson, M. Urbanik, H.-J. Völk, E. Waxman, J. Wefel, B. Wiebel-Sooth, R. Wielebinski and C. Wiebusch for inspiring discussions. JKB and JD would like to thank the IceCube collaboration for useful comments. Support for PLB is coming from the AUGER membership and theory grant 05 CU 5PD 1/2 via DESY/BMBF, as well as from VIHROS. Support for JKB is coming from the DFG grant BE-3714/3-1. Further, JD and JKB are supported by the IceCube grants BMBF (05 CI5PE1/0) and (05 A08PE1). Support for TMK is coming from the DFG grant Kn 765/1-2.

Appendix A: Catalog tables

We present the catalog of nearby starburst galaxies discussed throughout the paper. The 127 sources presented here were selected from a larger sample of 309 sources, all previously identified as starburst galaxies. We require the FIR flux at 60μ to be larger than $S_{60\mu} > 4$ Jy and the radio flux at 1.4 GHz to be larger than $S_{1.4\text{GHz}} > 20$ mJy. In addition, we only include sources at $z < 0.03$. Table A.1 summarizes the basic properties of the catalog: name, right ascension (RA [deg]), declination (DEC [deg]), redshift (z) and distance (D_L [Gpc]), together with the FIR flux measurements, S_λ , λ giving the wavelength. Table A.2 presents radio flux measurements, S_ν , with ν as the frequency. Table A.3 summarizes X-ray flux measurements. References are always given in the last column.

Table A.1. Coordinates, distances and IRAS measurements of the sample. All fluxes in [Jy]. Coordinates epoch J2000.0 and distances are obtained from NED. In NED, distances are corrected to the cosmological microwave background using cosmological parameters according to Λ CDM cosmology, $h_0 = 0.73$, $\Omega_m = 0.27$, $\Omega_\Lambda = 0.73$, using Wright (2006).

IRAS References:

1: Sanders et al. (2003), 2: Moshir et al. (1990b), 3: Lisenfeld et al. (2007), 4: Surace et al. (2004), 5: Knapp (1994), 6: Beichman et al. (1988), 7: Soifer et al. (1989)

Name	RA [deg]	DEC [deg]	z	D_L [Gpc]	$S_{12\mu m}$	$S_{25\mu m}$	$S_{60\mu m}$	$S_{100\mu m}$	References
MRK545	2.47254	25.9238	0.01523	0.05962	0.523	1.082	9.196	15.34	2
NGC34	2.77729	-12.1073	0.019617	0.0771	0.35	2.39	17.05	16.86	1
MCG-02-01-051	4.71202	-10.3768	0.027103	0.109	0.24	1.19	7.35	10.22	4
NGC174	9.24558	-29.4778	0.011905	0.0451	0.41	1.27	11.36	19.77	1
NGC232	10.6909	-23.5614	0.022172	0.0886	0.36	1.28	10.05	17.14	1
NGC253	11.888	-25.2882	0.0008	0.0031	41.04	154.67	967.81	1288.15	1
IC1623	16.9466	-17.507	0.02007	0.07857	1.03	3.65	22.93	31.55	1
NGC520	21.1461	3.79242	0.00761	0.03022	0.9	3.22	31.52	47.37	2
NGC632	24.323	5.87764	0.010567	0.0396	0.37	0.88	4.89	7.32	5
NGC660	25.7598	13.6457	0.00283	0.01233	3.05	7.3	65.52	114.74	1
NGC828	32.5399	39.1904	0.01793	0.07073	0.72	1.07	11.46	25.33	1
NGC891	35.6392	42.3491	0.00176	0.00857	5.27	7	66.46	172.23	1
NGC958	37.6785	-2.939	0.01914	0.0765	0.62	0.94	5.85	15.08	1
NGC1055	40.4385	0.443167	0.00332	0.01131	2.24	2.84	23.37	65.26	1
Maffei2	40.4795	59.6041	-5.7e - 05	0.00332	3.624	9.238	135	225	6
NGC1068(M77)	40.6696	-0.0132806	0.00379	0.0137	39.84	87.57	196.37	257.37	1
UGC2238	41.5729	13.0957	0.021883	0.0883	0.36	0.65	8.17	15.67	1
NGC1097	41.5794	-30.2749	0.00424	0.0152	2.96	7.3	53.35	104.79	1
NGC1134	43.4222	13.0141	0.012142	0.0474	0.55	0.92	9.09	19.43	1
NGC1365	53.4015	-36.1404	0.00546	0.01793	5.12	14.28	64.31	165.67	1
IC342	56.7021	68.0961	0.0001	0.0046	14.92	34.48	180.8	391.66	1
UGC02982	63.0935	5.54739	0.017696	0.0724	0.57	0.83	8.39	16.82	1
NGC1530	65.8629	75.2956	0.00821	0.03622	0.72	1.23	9.88	25.88	1
NGC1569	67.7044	64.8479	-0.00035	0.0046	1.24	9.03	54.36	55.29	1
MRK617	68.4994	-8.57888	0.01594	0.06261	0.441	7.286	32.31	32.69	1
NGC1672	71.4271	-59.2473	0.00444	0.01682	2.47	5.25	41.21	77.92	1
MRK1088	73.6598	3.26797	0.01528	0.06051	0.2659	0.835	6.605	10.77	1
NGC1808	76.9264	-37.5131	0.00332	0.01261	5.4	17	105.55	141.76	1
NGC1797	76.937	-8.01908	0.014814	0.0616	0.33	1.35	9.56	12.76	1
MRK1194	77.9423	5.20061	0.01491	0.05948	0.283	0.7071	6.688	11.5	2
NGC2146	94.6571	78.357	0.00298	0.012	6.83	18.81	146.69	194.05	1
NGC2276	111.81	85.7546	0.00804	0.0328	1.07	1.63	14.29	28.97	1
NGC2403	114.214	65.6026	0.00044	0.00247	2.82	3.57	41.47	99.13	1
NGC2415	114.236	35.242	0.01262	0.05341	0.61	1.19	8.75	13.58	1
NGC2782	138.521	40.1137	0.00848	0.03951	0.64	1.51	9.17	13.76	1
NGC2785	138.814	40.9175	0.008746	0.0392	0.49	1.09	8.4	15.79	1
NGC2798	139.346	41.9997	0.00576	0.02784	0.76	3.21	20.6	29.69	2
NGC2903	143.042	21.5008	0.00186	0.00826	5.29	8.64	60.54	130.43	1
MRK708	145.548	4.67314	0.00682	0.03116	0.46	0.8	5.36	8.24	1
NGC3034(M82)	148.968	69.6797	0.00068	0.00363	79.43	332.63	1480.42	1373.69	1
NGC3079	150.491	55.6797	0.00375	0.01819	2.54	3.61	50.67	104.69	1

Table A.1. continued.

Name	RA [deg]	DEC [deg]	z	D_L [Gpc]	$S_{12\mu m}$	$S_{25\mu m}$	$S_{60\mu m}$	$S_{100\mu m}$	References
NGC3147	154.224	73.4007	0.00941	0.04141	1.95	1.03	8.17	29.61	1
NGC3256	156.964	-43.9038	0.00935	0.03535	3.57	15.69	102.63	114.31	1
MRK33	158.133	54.401	0.00477	0.0221	0.21	1.05	4.77	5.99	5
NGC3310	159.691	53.5034	0.00331	0.01981	1.54	5.32	34.56	44.19	1
NGC3367	161.646	13.7509	0.010142	0.0468	0.51	1.98	6.44	13.48	1
NGC3448	163.663	54.3052	0.0045	0.02406	0.22	0.64	6.64	11.17	1
NGC3504	165.797	27.9725	0.00512	0.02707	1.11	4.03	21.43	34.05	1
NGC3556(M108)	167.879	55.6741	0.00233	0.01385	2.29	4.19	32.55	76.9	1
NGC3627(M66)	170.063	12.9915	0.00243	0.01004	4.82	8.55	66.31	136.56	1
NGC3628	170.071	13.5895	0.00281	0.01004	3.13	4.85	54.8	105.76	1
NGC3683	171.883	56.8771	0.005724	0.0259	1.16	1.48	13.87	29.3	1
NGC3690	172.134	58.5622	0.01041	0.04774	3.97	24.51	113.05	111.42	2
MRK188	176.893	55.9672	0.00803	0.0355	0.3621	0.4515	4.576	11.52	2
NGC3893	177.159	48.7108	0.00323	0.0161	1.45	1.65	15.57	36.8	1
NGC3994	179.404	32.2776	0.010294	0.0466	0.32	0.46	4.98	10.31	4
NGC4030	180.099	-1.1	0.00487	0.0245	1.35	2.3	18.49	50.92	1
NGC4041	180.551	62.1373	0.00412	0.02278	1.13	1.56	14.15	31.74	2
NGC4102	181.596	52.7109	0.002823	0.0141	1.77	6.83	46.85	70.29	1
MRK1466	182.046	2.87828	0.00443	0.01529	0.325	1.236	6.265	10.52	2
MRK759	182.656	16.0329	0.00723	0.0345	0.2995	0.537	4.116	8.727	2
NGC4194	183.539	54.5268	0.00834	0.04033	0.99	4.51	23.2	25.16	1
NGC4214	183.913	36.3269	0.00097	0.00367	0.58	2.46	17.57	29.08	2
NGC4273	184.984	5.34331	0.007932	0.0376	0.77	1.65	9.38	21.76	1
NGC4303(M62)	185.479	4.47365	0.005224	0.0264	3.28	4.9	37.27	78.74	1
NGC4414	186.613	31.2235	0.00239	0.01768	2.78	3.61	29.55	70.69	1
NGC4418	186.728	-0.877556	0.007268	0.0349	0.99	9.67	43.89	31.97	1
NGC4527	188.535	2.65381	0.005791	0.0286	2.65	3.55	31.4	65.68	1
NGC4536	188.613	2.18789	0.006031	0.0297	1.55	4.04	30.26	44.51	1
NGC4631	190.533	32.5415	0.00202	0.00773	5.16	8.97	85.4	160.08	1
NGC4666	191.286	-0.461885	0.005101	0.0257	3.34	3.89	37.11	85.95	1
NGC4793	193.67	28.9383	0.008286	0.038	1.08	1.57	12.42	28.11	1
NGC4826(M64)	194.182	21.6811	0.00136	0.0309	2.36	2.86	36.7	81.65	1
NGC4945	196.364	-49.4682	0.00187	0.00392	27.47	42.34	625.46	1329.7	1
NGC5005	197.734	37.0592	0.00316	0.01809	1.65	2.26	22.18	63.4	1
NGC5020	198.166	12.5998	0.011214	0.0507	0.36	0.72	5.58	11.7	1
NGC5055(M63)	198.956	42.0293	0.00168	0.00796	5.35	6.36	40	139.82	1
ARP193	200.147	34.1395	0.02335	0.101	0.25	1.42	17.04	24.38	1
NGC5104	200.346	0.342417	0.018606	0.082	0.39	0.74	6.78	13.37	1
NGC5135	201.434	-29.8337	0.01372	0.05215	0.63	2.38	16.86	30.97	1
NGC5194(M51)	202.47	47.1952	0.00154	0.00873	7.21	9.56	97.42	221.21	1
NGC5218	203.043	62.7678	0.009783	0.0419	0.37	0.94	7.01	13.54	1
NGC5236(M83)	204.254	-29.8657	0.00172	0.00363	21.46	43.57	265.84	524.09	1
NGC5256	204.573	48.2769	0.027863	0.119	0.32	1.07	7.25	10.11	1
NGC5257	204.968	0.839583	0.022676	0.099	0.52	1.18	8.1	13.63	4

Table A.1. continued.

Name	RA [deg]	DEC [deg]	z	D_L [Gpc]	$S_{12\mu m}$	$S_{25\mu m}$	$S_{60\mu m}$	$S_{100\mu m}$	References
NGC5253	204.983	-31.6401	0.00136	0.00315	2.612	12.07	29.84	30.08	2
UGC8739	207.308	35.2574	0.016785	0.0728	0.35	0.42	5.79	15.89	1
MRK1365	208.63	15.0441	0.01846	0.0806	0.1562	0.6445	4.203	6.113	2
NGC5430	210.191	59.3283	0.009877	0.0423	0.5	1.94	10.1	20.34	1
NGC5427	210.859	-6.03081	0.008733	0.0399	1.29	1.48	10.24	25.29	1
NGC5678	218.023	57.9214	0.00641	0.03202	0.94	1.2	9.67	25.66	1
NGC5676	218.195	49.4579	0.007052	0.0308	1.13	1.7	12.04	29.91	1
NGC5713	220.048	-0.289222	0.00658	0.02674	1.47	2.84	22.1	37.28	1
NGC5775	223.49	3.54446	0.00561	0.02634	1.83	2.47	23.59	55.64	1
NGC5900	228.772	42.2094	0.008376	0.0361	0.4	0.7	7.51	16.95	1
NGC5936	232.504	12.9893	0.013356	0.0575	0.48	1.47	8.73	17.66	1
ARP220	233.738	23.5032	0.01813	0.0799	0.61	8	104.09	115.29	1
NGC5962	234.132	16.6079	0.006528	0.0288	0.73	1.04	8.93	21.82	1
NGC5990	236.568	2.41547	0.012806	0.055	0.6	1.6	9.59	17.14	1
NGC6181	248.087	19.8266	0.007922	0.0334	0.63	1.41	8.94	20.83	1
NGC6217	248.163	78.1982	0.00454	0.02349	0.74	2.03	11.35	20.62	1
NGC6240	253.245	2.40094	0.02448	0.10336	0.59	3.55	22.94	26.49	1
NGC6286	254.631	58.9363	0.018349	0.0761	0.47	0.62	9.24	23.11	1
IRAS18293-3413	278.171	-34.191	0.01818	0.07776	1.14	3.98	35.71	53.38	1
NGC6701	280.802	60.6533	0.01323	0.05664	0.55	1.32	10.05	20.05	1
NGC6764	287.068	50.9332	0.008059	0.03131	0.54	1.33	6.62	12.44	1
NGC6946	308.718	60.1539	0.00016	0.00532	12.11	20.7	129.78	290.69	1
NGC7130	327.081	-34.9513	0.01615	0.06599	0.58	2.16	16.71	25.89	1
IC5179	334.038	-36.8437	0.01141	0.0467	1.18	2.4	19.39	37.29	1
NGC7331	339.267	34.4156	0.00272	0.01471	3.94	5.92	45	110.16	1
NGC7469	345.815	8.874	0.01632	0.06523	1.59	5.96	27.33	35.16	1
NGC7479	346.236	12.3229	0.00794	0.03236	1.37	3.86	14.93	26.73	1
NGC7496	347.447	-43.4279	0.0055	0.02234	0.58	1.93	10.14	16.57	1
NGC7541	348.683	4.53436	0.008969	0.032	1.52	2.09	20.08	41.87	1
IC5298	349.003	25.5567	0.027422	0.11	0.34	1.95	9.06	11.99	1
NGC7552	349.045	-42.5848	0.00536	0.02144	3.76	11.92	77.37	102.92	1
NGC7591	349.568	6.58581	0.016531	0.0636	0.28	1.27	7.87	14.87	1
NGC7592	349.592	-4.41694	0.024444	0.0972	0.26	0.97	8.05	10.58	1
MRK319	349.66	25.2329	0.027012	0.108	0.2211	0.5418	4.266	7.062	2
NGC7673	351.921	23.5889	0.01137	0.0422	0.1329	0.5165	4.98	6.893	1,2
NGC7678	352.116	22.4212	0.011639	0.0433	0.63	1.16	6.98	14.84	1
MRK534	352.194	3.51142	0.01714	0.0677	0.5	1.12	7.4	10.71	1
NGC7679	352.194	3.51142	0.017139	0.0662	0.5	1.12	7.58	10.71	1
NGC7714	354.059	2.15516	0.00933	0.0386	0.47	2.88	11.16	12.26	1
NGC7771	357.854	20.1118	0.01427	0.05711	0.99	2.17	19.67	40.12	1
NGC7793	359.458	-32.591	0.00076	0.0031	1.32	1.67	18.14	54.07	1
MRK332	359.856	20.7499	0.00802	0.0283	0.3598	0.6212	4.871	9.493	2

Table A.2. Radio measurements of the sample. All fluxes in [mJy].

References:
 1: Becker et al. (1991), 2: Condon et al. (2002), 3: Condon et al. (1983), 4: Condon et al. (1998), 5: Griffith et al. (1994), 6: Condon et al. (1996), 7: Wright et al. (1996), 8: Dressel & Condon (1978), 9: Gallimore et al. (2006), 10: Sramek (1975), 11: Bravo-Alfaro et al. (2004), 12: Rosa-González et al. (2007), 13: Griffith et al. (1995), 15: Vollmer et al. (2004), 16: Wright & Otrupcek (1990), 17: Kühr et al. (1981), 18: Wright et al. (1994), 19: White & Becker (1992), 20: Becker et al. (1995), 21: Strickland et al. (2004), 22: Nagar et al. (2005), 24: Disney & Wall (1977), 25: Leroy et al. (2005b), 26: Condon (1983), 27: Iono et al. (2005), 28: Sramek & Tovmassian (1976)

Name	S _{1.40 GHz}	S _{2.38 GHz}	S _{2.69 GHz}	S _{2.70 GHz}	S _{4.85 GHz}	S _{5.00 GHz}	S _{5.01 GHz}	References
MRK545	73.5	47	–	–	33	36	–	1, 2, 8, 14
NGC34	67.5	–	–	–	–	–	–	4
MCG-02-01-051	43.2	–	–	–	–	–	–	4
NGC174	45.7	–	–	–	–	–	–	4
NGC232	60.6	–	–	–	56	–	–	4
NGC253	6000	–	–	3520	2433	–	2580	5, 16, 17
IC1623	249.2	–	–	–	96	–	–	4, 5
NGC520	176	110	–	–	87	–	–	1, 2, 8
NGC632	23	15	–	–	–	–	–	2, 8
NGC660	373	255	–	–	187	–	–	1, 4, 8
NGC828	108	–	–	–	47	–	–	6
NGC891	701	–	–	–	342	–	–	2
NGC958	71.9	–	–	–	–	–	–	4
NGC1055	200.9	129	–	150	63	–	–	1, 4, 8, 16
Maffei2	1015	–	–	–	375	–	–	1, 19
NGC1068(M77)	4850	–	–	305	2039	1890	1342.4	2, 9, 13, 14, 17
UGC2238	72.2	–	–	–	–	–	–	1, 2
NGC1097	415	–	–	250	126	–	150	6, 7, 16
NGC1134	89.1	57	–	–	32	–	–	1, 2, 8
NGC1365	530	–	–	350	230	180	–	4, 7, 16
IC342	2250	–	–	–	277	–	–	1, 6
UGC02982	91.3	–	–	–	–	–	–	2
NGC1530	80.7	–	–	–	27	–	–	1, 6
NGC1569	396	–	–	–	198	–	155	1, 10, 19
MRK617	138	–	–	–	63	–	–	4, 13
NGC1672	450	–	–	210	114	–	100	16, 18
MRK1088	45.7	31	–	–	–	–	–	2, 8
NGC1808	497	–	–	350	229	–	220	6, 16, 18
NGC1797	29.1	–	–	–	–	–	–	4
MRK1194	42.2	27	–	–	–	–	–	2, 8
NGC2146	1087	–	–	–	–	–	–	6
NGC2276	283	–	–	–	–	–	–	6
NGC2403	387	–	–	–	169	–	–	19
NGC2415	66.4	53	–	–	41	–	30	1, 2, 8, 10
NGC2782	107.5	–	–	–	47	–	60	1, 10, 20
NGC2785	67.6	–	–	–	–	–	–	2
NGC2798	82.0	–	–	–	37	–	53	1, 2, 10
NGC2903	444	200	–	–	118	–	–	1, 2, 8, 13
MRK708	32.6	21	–	–	–	–	–	2, 8

Table A.2. continued.

Name	S _{1.40 GHz}	S _{2.38 GHz}	S _{2.69 GHz}	S _{2.70 GHz}	S _{4.85 GHz}	S _{5.00 GHz}	S _{5.01 GHz}	References
NGC3034(M82)	7286.8	–	5650	–	3918	–	3912	1, 17, 20
NGC3079	820.7	–	–	–	321	–	–	1, 21
NGC3147	89.9	–	–	–	44	–	8.1	1, 2, 23
NGC3256	642	–	–	–	319	240	250	5, 6, 14, 16
MRK33	24.6	–	–	–	–	–	–	11
NGC3310	417	–	–	–	152	–	–	1, 19
NGC3367	118	71	–	130	36	–	35	1, 2, 8, 10, 16
NGC3448	51.3	–	–	–	–	–	39	1, 10
NGC3504	274	–	–	–	117	–	–	1, 2, 8
NGC3556(M108)	245	–	–	–	76	–	–	1, 19
NGC3627(M66)	458	209	–	–	141	–	–	1, 2, 8
NGC3628	470.2	313	–	–	276	200	224	1, 8, 10, 14, 21
NGC3683	127	–	–	–	–	–	–	2
NGC3690	658	–	–	–	–	–	362	10, 23
MRK188	30.7	–	–	–	–	–	25.0	2, 10
NGC3893	139	–	–	–	39	–	–	1, 2
NGC3994	70.8	50	–	–	52	–	–	1, 2, 8
NGC4030	147	–	–	90	–	56	–	14, 16, 19
NGC4041	103	–	–	–	48	–	–	1, 2
NGC4102	273	–	–	–	70	–	105	1, 10
MRK1466	20.0	15	–	–	–	–	–	2, 8
MRK759	31.9	16	–	–	13	–	–	2, 8, 15
NGC4194	122	–	–	–	39	–	–	1, 19
NGC4214	38.3	–	–	–	30	–	–	2
NGC4273	78.5	65	–	–	37	–	–	2, 8, 15
NGC4303(M62)	444	195	–	–	102	120	–	2, 8, 14, 15
NGC4414	227	138	–	–	75	–	–	1, 8, 19
NGC4418	38.5	–	–	–	–	–	–	23
NGC4527	187.9	129	–	–	72	–	–	2, 8, 15
NGC4536	204.9	136	–	–	114	110	–	2, 8, 13
NGC4631	1122	340	–	–	438	–	–	1, 8, 19
NGC4666	434	–	–	–	161	–	–	2, 13
NGC4793	113	72	–	–	46	–	–	1, 2, 8
NGC4826(M64)	103	67	–	–	54	–	–	1, 2, 8
NGC4945	6600	–	–	5000	3055	–	2840	16, 18
NGC5005	194	–	–	–	62	–	–	1, 19
NGC5020	30.1	22	–	–	–	–	–	2, 8
NGC5055(M63)	349	–	–	–	124	–	–	1, 2
ARP193	104	–	–	–	53	–	–	1, 2
NGC5104	39.9	38	–	–	–	–	–	2, 8
NGC5135	194	–	–	–	107	–	–	6, 7
NGC5194(M51)	1310	–	–	–	436	–	360	1, 10, 19
NGC5218	30.4	–	–	–	–	–	–	2
NGC5236(M83)	2445	–	–	–	648	–	–	6, 7, 16

Table A.2. continued.

Name	S _{1.40 GHz}	S _{2.38 GHz}	S _{2.69 GHz}	S _{2.70 GHz}	S _{4.85 GHz}	S _{5.00 GHz}	S _{5.01 GHz}	References
NGC5256	159	–	–	–	47	–	–	1, 19
NGC5257	48.7	48	–	–	–	–	–	2, 8
NGC5253	83.8	–	–	–	90	75	–	6, 7, 14
UGC8739	93.6	–	–	–	37	–	–	1, 2
MRK1365	23.0	14	–	–	–	–	–	2, 8
NGC5430	65.9	–	–	–	29	–	40	1, 2, 10
NGC5427	63	–	–	–	–	–	–	26
NGC5678	110	–	–	–	68	–	–	2
NGC5676	116	–	–	–	38	–	33	2
NGC5713	222	–	–	–	93	73	–	1, 2, 14
NGC5775	221	138	–	–	67	–	–	1, 8, 19
NGC5900	60.4	–	–	–	–	17	–	2, 10
NGC5936	139	81	–	–	48	–	59	1, 2, 8, 10
ARP220	324	–	260	–	208	–	–	1, 2, 3
NGC5962	82.3	56	–	–	36	–	–	1, 2, 8
NGC5990	63.9	39	–	–	–	–	–	2, 8
NGC6181	95.6	60	–	–	56	–	–	1, 2, 8
NGC6217	79.9	–	–	–	–	–	–	2
NGC6240	653	–	–	–	179	–	170	13, 16, 19
NGC6286	157	–	–	–	53	–	–	1, 2
IRAS18293-3413	223	–	–	–	144	–	–	6, 7
NGC6701	92.2	–	–	–	22	–	–	1, 6
NGC6764	115.0	–	–	–	34	–	47	1, 2, 10
NGC6946	1395	–	–	–	531	–	–	1, 19
NGC7130	183	–	–	–	–	–	–	6
IC5179	165	–	–	–	79	–	–	6, 7
NGC7331	373	187	–	–	80	–	–	1, 2, 8
NGC7469	255	132	–	–	95	–	–	8, 13, 19
NGC7479	107	58	–	–	41	–	–	1, 2, 8
NGC7496	36.3	–	–	–	–	–	–	6
NGC7541	162	101	–	–	56	–	–	1, 2, 8
IC5298	24.2	–	–	–	–	–	–	23
NGC7552	276	–	–	–	139	–	–	6, 18
NGC7591	52.1	39	–	–	–	–	–	2, 8
NGC7592	75	–	–	–	–	–	–	27
MRK319	31.6	21	–	–	–	–	–	2, 8
NGC7673	43.4	30	–	–	–	–	–	2, 8
NGC7678	49.5	36	–	–	–	–	–	2, 8
MRK534	55.8	33	–	–	45	–	–	2, 8, 13
NGC7679	55.8	33	–	–	45	–	–	2, 8, 13
NGC7714	65.8	–	–	–	39	–	–	1, 2
NGC7771	229	97	–	–	57	–	–	1, 8, 19
NGC7793	103	–	–	–	–	–	–	6
MRK332	36.5	27	–	–	–	–	–	2, 8

Table A.3. X-Ray measurements of the sample. All fluxes in [nJy].

References:

1: Rigopoulou et al. (1996), 2: Fabbiano et al. (1992), 3: White et al. (2000), 4: Tajer et al. (2005), 5: Brinkmann et al. (1994), 6: Ott et al. (2005), 7: Tüllmann et al. (2006), 8: Teng et al. (2005), 9: Shu et al. (2007), 10: Guainazzi et al. (2005)

Name	EO IPC(ROSAT) 0.1-4 keV	EINSTEIN 0.2-4.0 keV	Chandra 0.1-2.4 keV	ROSAT 0.2-2.0 keV	ROSAT 0.1-2.4 keV	Chandra 0.3-8 keV	XMM 0.3-2 keV	References
NGC34	–	–	–	–	–	–	23	9
NGC520	–	–	–	33.4	–	–	–	3
NGC660	–	–	–	45.1	–	–	–	3
NGC891	–	–	–	–	–	–	69.4	7
NGC1068(M77)	–	3940	–	–	10900	–	–	2, 5
NGC1097	–	578	–	–	–	–	–	2
NGC1365	–	326	–	–	–	–	–	2
IC342	–	939	–	–	–	–	–	2
NGC1569	–	368	–	–	–	–	–	2
MRK617	–	124	–	–	–	–	–	2
MRK1088	–	–	–	42.3	–	–	–	8
NGC1808	–	–	–	–	446	–	–	5
NGC2403	–	364	–	–	–	–	–	2
NGC2415	–	–	–	63.8	–	–	–	3
NGC2903	–	273	–	46.4	–	–	–	2, 3
NGC3034(M82)	–	4490	–	–	–	–	–	2
NGC3079	–	113	–	–	–	–	–	2
NGC3256	–	–	–	–	1060	–	–	5
NGC3310	–	208	–	–	–	–	–	2
NGC3367	102	–	–	–	–	–	–	1
NGC3448	–	72.6	–	–	–	–	–	2
NGC3504	–	76.8	–	–	–	–	–	2
NGC3627(M66)	–	–	–	–	603	–	–	5
NGC3690	–	91.5	–	–	–	–	–	2
NGC4102	–	–	–	–	–	–	45.1	9
NGC4214	–	–	–	–	–	75.6	–	6
NGC4273	–	–	–	67.1	–	–	–	3
NGC4303(M62)	–	180	–	–	233	–	–	2, 5
NGC4536	–	112	–	–	–	–	–	2
NGC4631	–	263	–	–	–	–	–	2
NGC4826(M64)	–	150	–	53.3	–	–	–	3
NGC4945	–	–	–	–	794	–	–	5
NGC5135	–	63.9	–	176	–	–	–	3
NGC5236(M83)	–	972	–	–	954	–	–	2, 5
NGC5256	–	–	–	–	–	–	9.93	10
NGC5253	–	41.4	–	38.5	–	35.8	–	2, 3, 6
NGC5775	–	–	–	–	–	–	15.8	7
ARP220	45.69	–	–	–	–	–	–	1
NGC6240	–	–	–	–	914	–	–	5
NGC6946	–	611	–	–	–	–	–	2

Table A.3. continued.

Name	EO IPC(ROSAT) 0.1-4 keV	EINSTEIN 0.2-4.0 keV	Chandra 0.1-2.4 keV	ROSAT 0.2-2.0 keV	ROSAT 0.1-2.4 keV	Chandra 0.3-8 keV	XMM 0.3-2 keV	References
NGC7331	–	16.8	–	76.7	–	–	–	2, 3
NGC7469	–	12000	–	–	–	–	–	2
NGC7552	–	167	–	–	–	–	–	2
MRK534	–	204	–	–	–	–	–	3
NGC7679	–	204	–	–	–	–	–	2
NGC7714	–	53.8	–	–	–	–	–	2
NGC7771	–	138	–	–	–	–	–	2
NGC7793	–	130	–	–	–	–	–	2

References

- Achterberg, A. 1979, *Astron. & Astroph.*, 76, 276
- Achterberg, A., (IceCube Coll.), et al. 2007, *Astroph. J.*, 664, 397
- Achterberg, A., (IceCube Coll.), et al. 2008, *Astroph. J.*, 674, 357
- Ahrens, J., (IceCube Coll.), et al. 2004, *Astropart. Phys.*, 20, 507
- Anchordoqui, L. A. et al. 2008, *Astropart. Phys.*, 29, 1
- Appenzeller, I. 1974, *Astron. & Astroph.*, 36, 99
- Ave, M. et al. 2005, *Astropart. Phys.*, 23, 19
- Baade, W. & Zwicky, F. 1934, *Proc. Nat. Acad. Science*, 20, 259
- Baan, W. A. & Klöckner, H.-R. 2006, *Astron. & Astroph.*, 449, 559
- Bartel, N. et al. 1987, *Astroph. J.*, 323, 505
- Beck, R. & Hoernes, P. 1996, *Nature*, 379, 47
- Beck, R. et al. 1996, *Ann. Rev. Astron. Astrophys.*, 34, 155
- Beck, R. et al. 2003, *A&A*, 411, 99
- Becker, J. K. et al. 2006, *Astropart. Phys.*, 25, 118
- Becker, R. H., White, R. L., & Edwards, A. L. 1991, *Astroph. J. Suppl. Series*, 75
- Becker, R. H., White, R. L., & Helfland, D. J. 1995, *Astroph. J.*, 450
- Bednarz, J. & Ostrowski, M. 1998, *Phys. Rev. Lett.*, 80, 3911
- Beichman, C. A. et al., eds. 1988
- Bell, A. R. 2004, *Mon. Not. Roy. Astron. Soc.*, 353, 550
- Bell, A. R. 2005, *Mon. Not. Roy. Astron. Soc.*, 358, 181
- Berezinsky, V. S. et al. 1990, North-Holland, Amsterdam
- Berger, E. et al. 2003, *Nature*, 426, 154
- Beuermann, K., Kanbach, G., & Berkhuijsen, E. M. 1985, *Astron. & Astroph.*, 153, 17
- Bicay, M. D. et al. 1989, *Astroph. J. Lett.*, 338, L53
- Biermann, L. 1950, *Z. f. Naturf.*, 5a, 65
- Biermann, L. & Schlüter, A. 1951, *Physics Reviews*, 82, 863
- Biermann, P., Eckart, A., & Witzel, A. 1985, *Astron. & Astroph.*, 142, L23
- Biermann, P. & Fricke, K. 1977, *Astron. & Astroph.*, 54, 461
- Biermann, P. L. 1976, *Astron. & Astroph.*, 53, 295
- Biermann, P. L. 1995, in *Jubilee Gamow Seminar*, St. Petersburg, Vol. 74 (Kluwer Acad. Publ.), 385
- Biermann, P. L. 1998, in *Nuclear Astrophysics meeting*, Hirschegg, GSI, Darmstadt, 211
- Biermann, P. L. 2006, *IOP Journ. of Phys.: Conf. Ser.*, 47, 78
- Biermann, P. L. & Strom, R. 1993, *Astron. & Astroph.*, 275, 659
- Biermann, P. L. et al. 2001, *Astron. & Astroph.*, 369, 269
- Biermann, P. L. et al. 2008, in *Cosmic Ray International Seminar (CRIS)*, ed. A. Insolina, Malfa (Salina Island - Italy), arXiv: 0811.1848
- Bisnovatyi-Kogan, G. S., Ruzmaikin, A. A., & Syunyaev, R. A. 1973, *Soviet Astronomy*, 17, 137, translated from *Astron. Zh.*, 50:210 (1973)
- Bowyer, S. et al. 1995, *Nature*, 375, 212
- Bravo-Alfaro, H. et al. 2004, *Astron. J.*, 127, 264
- Breitschwerdt, D. 2008, *Nature*, 452, 826
- Breitschwerdt, D. & Schmutzler, T. 1994, *Nature*, 371, 774
- Brinkmann, W., Siebert, J., & Boller, T. 1994, *Astron. & Astroph.*, 281, 355
- Brunetti, M. T. & Codino, A. 2000, *Astroph. J.*, 528, 789
- Bykov, A. M. & Toptygin, I. N. 2005, *Astronomy Letters*, 31, 748, translation from *Pis'ma v Astron. Zh.*, 31:839 (2005)
- Cappellaro, E. & Turatto, M. 2001, in *Astrophysics and Space Science Library*, Vol. 264, *The Influence of Binaries on Stellar Population Studies*, ed. D. Vanbeveren, 199, arXiv:astro-ph/0012455
- Chini, R., Kreysa, E., & Biermann, P. L. 1989, *Astron. & Astroph.*, 219, 87
- Chyży, K. T. & Beck, R. 2004, *Astron. & Astroph.*, 417, 541
- Chyży, K. T. et al. 2000a, *Astron. & Astroph.*, 355, 128
- Chyży, K. T. et al. 2000b, *Astron. & Astroph.*, 356, 757
- Chyży, K. T. et al. 2006, *Astron. & Astroph.*, 447, 465
- Chyży, K. T. et al. 2007, *Astron. & Astroph.*, 462, 933
- Condon, J. J. 1983, *Astroph. J. Suppl. Series*, 53, 459
- Condon, J. J., Cotton, W. D., & Broderick, J. J. 2002, *Astron. J.*, 124, 675
- Condon, J. J. et al. 1983, *Astron. J.*, 88, 20
- Condon, J. J. et al. 1991, *Astroph. J.*, 376, 95x
- Condon, J. J. et al. 1996, *Astroph. J. Suppl. Series*, 103
- Condon, J. J. et al. 1998, *Astron. J.*, 115
- Connaughton, V. 2007, in *GRB conference*, Santa Fe
- Cox, D. P. 1972, *Astroph. J.*, 178, 159
- Cox, D. P. & Smith, B. W. 1974, *Astroph. J. Lett.*, 189, L105
- Cox, P. & Mezger, P. G. 1989, *AAR*, 1, 49
- de Avillez, M. & Breitschwerdt, D. 2004, *Astrophys. & Space Science*, 292, 207
- de Avillez, M. A. & Breitschwerdt, D. 2007, *Astroph. J. Lett.*, 665, L35
- de Jong, T. et al. 1985, *Astron. & Astroph.*, 147, L6
- Disney, M. J. & Wall, J. V. 1977, *Mon. Not. Roy. Astron. Soc.*, 179, 235
- Domingo-Santamaría, E. & Torres, D. F. 2005, *Astron. & Astroph.*, 444, 403
- Dopita, M. A. & Sutherland, R. S. 2003, *Astrophysics of the diffuse universe* (*Astrophysics of the diffuse universe*, Berlin, New York: Springer, 2003. Astronomy and astrophysics library, ISBN 3540433627)
- Dopita, M. A. et al. 2005, *Astroph. J.*, 619, 755
- Dopita, M. A. et al. 2006a, *Astroph. J.*, 647, 244
- Dopita, M. A. et al. 2006b, *Astroph. J. Suppl. Series*, 167, 177
- Douglas, J. N. et al. 1996, *Astron. J.*, 111
- Dressel, L. L. & Condon, J. J. 1978, *Astroph. J. Suppl. Series*, 36, 53
- Drury, L. O. 1983, *Rep. Prog. Phys.*, 46, 973
- Engelmann, J. J. et al. 1990, *Astron. & Astroph.*, 233, 96
- Everett, J. E. et al. 2008, *Astroph. J.*, 674, 258
- Fabbiano, G., Kim, D.-W., & Trinchieri, G. 1992, *Astroph. J. Suppl. Series*, 80, 531
- Fermi, E. 1949, *Phys. Rev.*, 75, 1169
- Ferrière, K. 1996, *Astron. & Astroph.*, 310, 438
- Ferrière, K. & Schmitt, D. 2000, *Astron. & Astroph.*, 358, 125
- Field, G. B. 1965, *Astroph. J.*, 142, 531
- Galante, N. et al. 2008, in *American Institute of Physics Conference Series*, Vol. 1000, *American Institute of Physics Conference Series*, ed. M. Galassi, D. Palmer, & E. Fenimore, 125
- Gallimore, J. F. et al. 2006, *Astron. J.*, 132, 546
- Goldstein, M. L., Roberts, D. A., & Matthaues, W. H. 1995, *Ann. Rev. Astron. Astrophys.*, 33, 283
- Gressel, O. et al. 2008, *Astron. & Astroph.*, 486, L35
- Griffith, M. R., Wright, A. E., Burke, B. F., & Ekers, R. D. 1995, *Astroph. J. Suppl. Series*, 97, 347
- Griffith, M. R. et al. 1994, *Astroph. J. Suppl. Series*, 90, 179
- Groves, B. et al. 2008, *Astroph. J. Suppl. Series*, 176, 438
- Guainazzi, M., Matt, G., & Perola, G. C. 2005, *Astron. & Astroph.*, 444, 119
- Guetta, D. et al. 2004, *Astropart. Phys.*, 20, 429
- Hanasz, M. et al. 2004, *Astroph. J. Lett.*, 605, L33
- Hanasz, M. et al. 2006, *Astronomische Nachrichten*, 327, 469
- Heeschen, D. S. & Wade, C. M. 1964, *Astron. J.*, 69
- Heisenberg, W. 1948, *Zeitschrift für Physik*, 124, 628
- Helou, G. et al. 1988, *Astroph. J. Suppl. Series*, 68, 151
- Hooper, D., Taylor, A., & Sarkar, S. 2005, *Astropart. Phys.*, 23, 11
- Hummel, E. & Beck, R. 1995, *Astron. & Astroph.*, 303, 691
- Hunter, S. D. et al. 1997, *Astroph. J.*, 481, 205
- Iono, D., Yun, M. S., & Ho, P. T. P. 2005, *Astroph. J. Suppl. Series*, 158, 1
- Kappes, A., (IceCube Coll.), et al. 2008, in *PANIC 2008*, Eilat, Israel
- Kardashev, N. S. 1962, *Astronomicheskii Zhurnal*, 39, 393, engl. transl. in *Sov. Astr.*, 6:317 (1962)
- Karlsson, N. 2008, arXiv:0810.0275
- Karman, v. T. & Howarth, L. 1938, in *A*, Vol. 164, *Roy. Soc. London*, 192
- Kelner, S. R., Aharonian, F. A., & Bugayov, V. V. 2006, *Phys. Rev. D*, 74, 034018
- Knapp, J. 1994, *Private Communication*
- Kneiske, T. M. & Mannheim, K. 2008, *Astron. & Astroph.*, 479, 41
- Kneiske, T. M., Mannheim, K., & Hartmann, D. H. 2002, *Astron. & Astroph.*, 386, 1
- Kolmogorov, A. N. 1941a, *Dokl. Akad. Nauk SSSR*, 30, 299
- Kolmogorov, A. N. 1941b, *Dokl. Akad. Nauk SSSR*, 31, 538
- Kolmogorov, A. N. 1941c, *Dokl. Akad. Nauk SSSR*, 32, 19
- Kowal, G., Hanasz, M., & Otmianowska-Mazur, K. 2003, *Astron. & Astroph.*, 404, 533
- Kowal, G., Otmianowska-Mazur, K., & Hanasz, M. 2006, *Astron. & Astroph.*, 445, 915
- Kraichnan, R. H. 1965, *Phys. of Fluids*, 8, 1385
- Kronberg, P. P. & Biermann, P. 1981, *Astroph. J.*, 243, 89
- Kronberg, P. P., Biermann, P., & Schwab, F. R. 1985, *Astroph. J.*, 291, 693
- Kronberg, P. P. & Sramek, R. A. 1985, *Science*, 227, 28
- Kronberg, P. P. et al. 2007, *Astroph. J.*, 659, 267
- Kühr, H. et al. 1981, *Astron. & Astroph. Suppl.*, 45, 367
- Kulsrud, R. M. 1999, *ARA&A*, 37, 37
- Kulsrud, R. M. & Zweibel, E. G. 2008, *Reports on Progress in Physics*, 71, 046901
- Lee, H. et al. 2003, *Astroph. J.*, 594, 627
- Leroy, A. et al. 2005a, *Astroph. J.*, 625
- Leroy, A. et al. 2005b, *Astroph. J.*, 625, 763
- Lisenfeld, U., Völk, H. J., & Xu, C. 1996, *Astron. & Astroph.*, 306, 677
- Lisenfeld, U. et al. 2007, *Astron. & Astroph.*, 462, 507
- Loeb, A. & Waxman, E. 2006, *J. Cosm. and Astr. Phys.*, 5, 3
- Lucek, S. G. & Bell, A. R. 2000, *Mon. Not. Roy. Astron. Soc.*, 314, 65
- Mannheim, K. & Schlickeiser, R. 1994, *Astron. & Astroph.*, 286, 983
- Mannucci, F. et al. 2003, *Astron. & Astroph.*, 401, 519
- Mazzali, P. A. et al. 2003, *Astroph. J. Lett.*, 599, L95
- McIvor, I. 1977, *Mon. Not. Roy. Astron. Soc.*, 178, 85
- McKee, C. F. & Ostriker, J. P. 1977, *Astroph. J.*, 218, 148
- Meli, A., Becker, J. K., & Quenby, J. J. 2008, *Astron. & Astroph.*, 492, 323
- Mezger, P. G. & Henderson, A. P. 1967, *Astroph. J.*, 147, 471
- Montaruli, T., (IceCube Coll.), et al. 2007, in *Topics in Astroparticle and*

- Underground Physics (TAUP), Sendai, Japan, arXiv:0712.3524
- Morsony, B. J., Lazzati, D., & Begelman, M. C. 2007, *Astron. J.*, 665, 569
- Moshir, M., Kopan, G., et al. 1990a, *Bullet. American Astron. Soc.*, 22
- Moshir, M., Kopan, G., et al. 1990b, *Bulletin of the American Astronomical Society*, 22
- Münich, K. 2007, PhD thesis, University of Technology, Dortmund
- Münich, K. et al. 2007, in 30th International Cosmic Ray Conference, ArXiv:711.0353
- Nagar, N. M., Falcke, H., & Wilson, A. S. 2005, *Astron. & Astroph.*, 435, 521
- Obukhov, A. M. 1941, *Dokl. Akad. Nauk SSSR*, 32, 22
- Otmianowska-Mazur, K. et al. 2008, *ApJ*, in press, arXiv:0812.2150
- Ott, J., Walter, F., & Brinks, E. 2005, *Mon. Not. Roy. Astron. Soc.*, 358, 1423
- Paglionone, T. A. D. et al. 1996, *Astron. J.*, 460, 295
- Parker, E. N. 1965, *Astron. J.*, 142, 584
- Parker, E. N. 1969, *Astron. J.*, 157, 1129
- Parker, E. N. 1992, *Astron. J.*, 401, 137
- Pavlidou, V. & Fields, B. D. 2002, *Astron. J. Lett.*, 575, L5
- Prandtl, L. 1925, *Z. angew. Math. & Mech.*, 5, 136
- Ptuskin, V. 1999, in International Cosmic Ray Conference, Vol. 4, International Cosmic Ray Conference, 291
- Racusin, J. L. et al. 2008, *Nature*, 455, 183
- Rickett, B. J. 1977, *Ann. Rev. Astron. Astrophys.*, 15, 479
- Rigopoulou, D., Lawrence, A., & Rowan-Robinson, M. 1996, *Mon. Not. Roy. Astron. Soc.*, 278, 1049
- Rodríguez-Pascual, P. M. et al. 1993, *Astrophys. & Space Science*, 205, 113
- Rosa-González, D. et al. 2007, *Astron. J.*, 654, 226
- Rybicki, G. B. & Lightman, A. P. 1979, *Radiative processes in astrophysics* (J. Wiley & Sons, Inc.)
- Sagdeev, R. Z. 1979, *Rev. Mod. Phys.*, 51, 1
- Sanders, D. B. et al. 2003, *Astron. J.*, 126, 1607
- Schmutzler, T. & Tscharnuter, W. M. 1993, *Astron. & Astroph.*, 273, 318
- Sedov, L. I. 1958, *Reviews of Modern Physics*, 30, 1077
- Shklovskii, I. S. 1953, *Dokl. Akad. Nauk, SSSR*, 91, 475, lib. of Congress Transl. RT-1495
- Shu, X. W. et al. 2007, *Astron. J.*, 657, 167
- Sinnis, G., Smith, A., & McEnery, J. E. 2005, in 10th Marcel Grossmann Meeting, 1068
- Smith, A. et al. 2006, in TeV Particle Astrophysics II, <http://icecube.wisc.edu/tev/presentations.php>
- Snowden, S. L. et al. 1997, *Astron. J.*, 485, 125
- Soifer, B. T., Boehmer, L., Neugebauer, G., & Sanders, D. B. 1989, *Astron. J.*, 98, 766
- Sramek, R. 1975, *Astron. J.*, 80, 771
- Sramek, R. A. & Tovmassian, H. M. 1976, *Astron. J.*, 207, 725
- Sreekumar, P. et al. 1998, *Astron. J.*, 494, 523
- Stamatikos, M., (IceCube Coll.), et al. 2005, International Conference of Cosmic Rays, Pune (India), arXiv:astro-ph/0510336
- Stanev, T., Biermann, P. L., & Gaisser, T. K. 1993, *Astron. & Astroph.*, 274, 902
- Stecker, F. W. 2007, *Astropart. Phys.*, 26, 398
- Stecker, F. W., Baring, M. G., & Summerlin, E. J. 2007, *Astron. J. Lett.*, 667, L29
- Stepanian, N. N. et al. 2008, *Solar System Research*, 42, 83
- Strickland, D. K. et al. 2004, *Astron. J.*, 606, 829
- Strong, A. W., Moskalenko, I. V., & Reimer, O. 2005, in AIP Conf. Proc. 745: High Energy Gamma-Ray Astronomy, 585
- Surace, J. A., Sanders, D. B., & Mazzearella, J. M. 2004, *Astron. J.*, 127, 3235
- Sutherland, R. S. & Dopita, M. A. 1993, *Astron. J. Suppl. Series*, 88, 253
- Tabatabaei, F. S., Krause, M., & Beck, R. 2007a, *Astron. & Astroph.*, 472, 785
- Tabatabaei, F. S. et al. 2007b, *Astron. & Astroph.*, 475, 133
- Tajer, M. et al. 2005, *Astron. & Astroph.*, 435, 799
- Teng, S. H. et al. 2005, *Astron. J.*, 633, 664
- Thompson, T. A., Quataert, E., & Waxman, E. 2007, *Astron. J.*, 654, 219
- Thompson, T. A. et al. 2006, arXiv:astro-ph/0608699
- Tüllmann, R. et al. 2006, *Astron. & Astroph.*, 448, 43
- van Buren, D. & Greenhouse, M. A. 1994, *Astron. J.*, 431, 640
- Vasileiou, V. & (MILAGRO Coll.) 2007, in GRB conference, Santa Fe
- Vietri, M. 1995, *Astron. J.*, 453, 883
- Völk, H. J. 1989, *Astron. & Astroph.*, 218, 67
- Volkova, L. V. 1980, *Sov. J. of Nucl. Phys.*, 31, 748
- Vollmer, B., Thierbach, M., & Wielebinski, R. 2004, *Astron. & Astroph.*, 418, 1
- Waxman, E. 1995, *Phys. Rev. Lett.*, 75, 386
- Waxman, E. & Bahcall, J. N. 1997, *Phys. Rev. Lett.*, 78, 2292
- Waxman, E. & Bahcall, J. N. 1999, *Phys. Rev. D*, 59, 23002
- Weibel, E. S. 1959, *Phys. Rev. Lett.*, 2, 83
- Westmeier, T., Brüns, C., & Kerp, J. 2005, *Astron. & Astroph.*, 432, 937
- White, N. E., Giommi, P., & Angelini, L. 2000, *VizieR Online Data Catalog*, 9031, 0
- White, R. L. & Becker, R. H. 1992, *Astron. J. Suppl. Series*, 79
- Whiteoak, J. B. 1970, 5, 29
- Wiebel-Sooth, B., Biermann, P. L., & Meyer, H. 1995, in International Cosmic Ray Conference, Vol. 3, International Cosmic Ray Conference, 45
- Wiebel-Sooth, B. & Biermann, P. L. 1999 (Springer Publ. Comp.), vol. VI/3c, 37. Invited Chapter for Landolt-Börnstein
- Wiebel-Sooth, B., Biermann, P. L., & Meyer, H. 1998, *Astron. & Astroph.*, 330, 389
- Wright, A. & Otrupcek, R. 1990, Australia Telescope National Facility
- Wright, A. E. et al. 1994, *Astron. J. Suppl. Series*, 91, 111
- Wright, A. E. et al. 1996, *Astron. J. Suppl. Series*, 103, 145
- Wright, E. L. 2006, The Publications of the Astronomical Society of the Pacific, 118, 1711
- Wunderlich, E. & Klein, U. 1988, *Astron. & Astroph.*, 206, 47
- Wunderlich, E. & Klein, U. 1991, *Astron. & Astroph. Suppl.*, 87, 247
- Wunderlich, E., Wielebinski, R., & Klein, U. 1987, *Astron. & Astroph. Suppl.*, 69, 487
- Xu, C., Lisenfeld, U., & Völk, H. J. 1994a, *Astron. & Astroph.*, 285, 19
- Xu, C. et al. 1994b, *Astron. & Astroph.*, 282, 19